

Modeling of PAHs From Global to Regional Scales: Model Development (IAP-AACM_PAH v1.0) and Investigation of Health Risks in 2013 and 2018 in China

Zichen Wu^{1,2,3}, Xueshun Chen^{1,2,3*}, Zifa Wang^{1,2,3*}, Huansheng Chen^{1,2,3}, Zhe Wang^{1,2,3}, Qing Mu⁴, Lin Wu^{1,2,3}, Wending Wang^{1,2,3}, Xiao Tang^{1,2,3}, Jie Li^{1,2,3}, Ying Li^{1,2,3}, Qizhong Wu⁵, Yang Wang^{3,6}, Zhiyin Zou^{1,2,3}, Zijian Jiang^{1,2,3}

¹ State Key Laboratory of Atmospheric Boundary Layer Physics and Atmospheric Chemistry, Institute of Atmospheric Physics, Chinese Academy of Sciences, Beijing 100029, China

² Key Laboratory of Atmospheric Environment and Extreme Meteorology, Institute of Atmospheric Physics, Chinese Academy of Sciences, Beijing 100029, China

³ University of Chinese Academy of Sciences, Beijing 100049, China

⁴ Department of Health and Environmental Sciences, School of Science, Xi'an Jiaotong-Liverpool University, Suzhou 215123, China

⁵ Beijing Normal University, Beijing 100875, China

⁶ Research Center for Eco-Environmental Sciences, Chinese Academy of Sciences, Beijing 100085, China

Correspondence to: Xueshun Chen (chenxsh@mail.iap.ac.cn) and Zifa Wang (zifawang@mail.iap.ac.cn)

Abstract. Polycyclic aromatic hydrocarbons (PAHs) significantly impact human health due to their persistence, toxicity, and potential carcinogenicity. Their global distribution and regional changes caused by emission changes, especially over areas in developing countries, remain to be understood along with their health impacts. This study implemented a PAH module in the global-regional nested Atmospheric Aerosol and Chemistry Model (IAP-AACM) to investigate the global distribution of PAHs and the change in their health risks from 2013 to 2018 in China. An evaluation against observations showed that the model could capture well the spatial distribution and seasonal variation of Benzo[a]pyrene (BaP), the typical indicator species of PAHs. At a global scale, the annual mean concentrations are highest in China, followed by Europe and India, with high values exceeding the target values of 1 ng m⁻³ over some areas. Compared with 2013, the concentration of BaP in China decreased in 2018 due to emission reductions, whereas it increased in India and Southern Africa. However, the decline is much smaller than for PM_{2.5} during the same period. The concentration of BaP decreased by 8.5% in Beijing-Tianjin-Hebei (BTH) and 9.4% in the Yangtze River Delta (YRD). It even increased over areas in the Sichuan Basin due to changes in meteorological conditions. The total incremental lifetime cancer risk (ILCR) posed by BaP

32 only showed a slight decrease in 2018 and the population in East China still faced significant potential
33 health risks. The results indicate that strict additional control measures should be taken to reduce the
34 pollution and health risks of PAHs effectively. The study also highlights the importance of considering
35 changes in meteorological conditions when evaluating emission changes from concentration monitoring.

36 **1 Introduction**

37 Polycyclic aromatic hydrocarbons (PAHs) are aromatic compounds with two or more aromatic rings.
38 PAHs have been categorized as persistent organic pollutants (POPs) by the United Nations Economic
39 Commission for Europe's (UNECE's) Convention on Long-Range Transboundary Air Pollution
40 (CLRTAP) (Friedman and Selin, 2012), and they are widely distributed in the environment through
41 atmospheric transport. PAHs have attracted significant attention in environmental research and risk
42 assessment due to their persistence, toxicity, and potential carcinogenicity (Chen and Liao, 2006; Shen
43 et al., 2014). These compounds are generated from both natural and anthropogenic sources (Haritash and
44 Kaushik, 2009). Volcanic eruption, forest, and prairie fire are the major natural sources of atmospheric
45 PAHs (Baek et al., 1991). Anthropogenic sources are the most important source of PAHs, including
46 incomplete combustion of fossil fuels and biomass (Li et al., 2022; Ravindra et al., 2008).

47 Understanding the sources, distribution, and fate of PAHs is crucial for assessing their impacts on
48 human health and the environment. Upon emission into the atmosphere, PAHs are redistributed by gas-
49 particulate partitioning, gaseous-phase reactions, heterogeneous reactions, air-soil exchange, and wet/dry
50 deposition during long-range transport (LRT, Inomata et al., 2013). Monitoring is the most commonly
51 used way to investigate the concentration of PAHs in the atmosphere. Due to the high costs of observation
52 and technical limitations, it is difficult to conduct a long-term and broad regional analysis through
53 monitoring (Zhen, 2023). Up to now, there are few continuous observations over the major continents at
54 the same time (Dong et al., 2023). A transport model is an effective tool to simulate the distribution of
55 PAHs and their LRT, which can greatly enhance our understanding of the distribution of PAHs on a
56 regional and global scale (Byun and Schere, 2006; Wang et al., 2021).

57 As recently outlined by Galarnau et al. (2014), several numerical modeling studies have been
58 reported in the literature. The models that can simulate PAHs include but are not limited to the following
59 examples, GEOS-Chem (Friedman et al., 2014; Friedman and Selin, 2012), ECHAM5 (Lammel and

60 Sehili, 2007; Lammel et al., 2009; Lammel et al., 2015; Octaviani et al., 2019), CAM5 (Lou et al., 2023;
61 Shrivastava et al., 2017), and MOZART-4 (Shen et al., 2014). The horizontal resolutions of these reported
62 models are primarily at $4^{\circ} \times 5^{\circ}$ and $2.8^{\circ} \times 2.8^{\circ}$. Shen et al. (2014) simulated the transport of
63 Benzo[a]pyrene (BaP), one of the most toxic and highly carcinogenic PAHs, in the global troposphere
64 based on MOZART-4, and they showed that the model resolution was crucial for the health risks
65 assessment. Lammel et al. (2015) demonstrated the significant impact of gas-particle partitioning
66 mechanisms on the atmospheric lifetime, compartment distributions, and LRT of PAHs. The regional
67 modeling studies focusing on Europe, East Asia, and North America have also been reported, with
68 horizontal resolutions ranging mainly from $54 \text{ km} \times 54 \text{ km}$ to $24 \text{ km} \times 24 \text{ km}$ (CMAQ (Aulinger et al.,
69 2009; Aulinger et al., 2007; Bieser et al., 2012; San José et al., 2013; Efstathiou et al., 2016), WRF-Chem
70 (Mu et al., 2018), AURAMS (Galarneau et al., 2014), and CanMETO (Zhang et al., 2011a; Zhang et al.,
71 2011b; Zhang et al., 2009)). Efstathiou et al. (2016) showed that considering absorption and adsorption
72 processes can better capture the concentration levels and seasonal variations of BaP. In recent years, the
73 effect of the heterogeneous reaction process of PAHs on transportation has also been studied. Mu et al.
74 (2018) developed a new kinetic scheme describing the effects of temperature and humidity on the organic
75 aerosol coating of BaP and BaP reaction rate. They found that low temperature and low humidity can
76 significantly increase the lifetime of BaP and enhance its LRT capacity.

77 However, the resolutions and spatial range differed greatly between these models. Most of the
78 models are either global or regional. There is a lack of simulation studies focusing on both global and
79 key regions, making it difficult to investigate a specific focus in a global background in a consistent
80 manner. Additionally, the resolution of most global models is low, which will further affect the health
81 risk assessment of PAHs. Furthermore, the up-to-date mechanisms (gas-particle partitioning,
82 heterogeneous reaction, and air-soil exchange) established for PAHs simulations are not considered in
83 earlier modeling studies.

84 China is one of the largest PAH-emitting countries in the world (Inomata et al., 2012; Zhang and
85 Tao, 2009). High concentrations of BaP have been reported (Bieser et al., 2012; Liu et al., 2014;
86 Shrivastava et al., 2017; Su et al., 2023). Over the polluted regions in eastern China, annual
87 concentrations of BaP exceeded 1 ng m^{-3} , the target values proposed in the European Union (EU) and
88 China. To improve air quality and protect public health, the State Council of China promulgated “the

89 Action Plan on Air Pollution Prevention and Control” (the Action Plan) in 2013. This Action Plan
90 established many effective emission reduction and energy-saving policies, such as strengthening
91 industrial emission standards, eliminating outdated polluting industries, upgrading industrial boilers, and
92 developing clean fuels in the residential sector. Since then, many studies have investigated the changes
93 in concentration levels and health risks of conventional pollutants, such as PM_{2.5} (Feng et al., 2019; Wang
94 et al., 2018; Zhang et al., 2019; Zhu et al., 2021; Wang et al., 2019). Wang et al. (2019) pointed out that
95 the annual average concentrations of PM_{2.5} in the Beijing-Tianjin-Hebei (BTH), the Yangtze River Delta
96 (YRD), and the Pearl River Delta (PRD) all decreased by more than 27% in 2017, indicating that the
97 control measures have achieved remarkable effects and the air quality has been significantly improved.
98 However, for non-conventional pollutants, such as BaP and other PAHs, their concentration changes due
99 to emission reduction in China after implementing of policies have not been quantified. The changes in
100 health risks and the benefits from control measures were not yet assessed.

101 Considering the aforementioned, we simulated PAHs from global to regional scales by coupling the
102 key physical and chemical modules associated with PAHs in a global-regional nested atmospheric
103 transport model. In particular, newly established parametrizations of gas-particle partitioning and
104 heterogeneous reaction were incorporated into the model. Then the changes in global concentration and
105 health risks of BaP over China were quantified based on model evaluation against a collected observation
106 dataset. The study can advance our understanding of global PAHs distribution and regional health risks
107 and their responses to emission change. The paper is arranged as follows: Section 2 briefly describes the
108 host model (IAP-AACM), the physical and chemical modules related to PAHs, and the method of
109 assessing health risks. Section 3 presents the configuration of the model and the observations used in the
110 evaluation. Section 4 shows the global and regional distributions of BaP concentrations and analyzes the
111 health risks associated with BaP in China. Section 5 discusses the uncertainty of the model. In Sect. 6,
112 the main conclusions are summarized.

113 **2 Model description and development**

114 **2.1 Description of host model**

115 The model used in this study is the Atmospheric Aerosol and Chemistry Model developed by the
116 Institute of Atmospheric Physics, Chinese Academy of Sciences (IAP-AACM) (Wei et al., 2019), which

117 was developed based on the Global Nested Air Quality Prediction Modeling System (GNAQPMS, Chen
118 et al., 2015; Wang et al., 2001). IAP-AACM is a 3-D Eulerian transport model that uses a multi-scale
119 domain-nesting approach to simulate atmospheric chemistry and aerosol processes from global to
120 regional scales. As recently described by Chen et al. (2015), compared with the traditional multi-scale
121 modeling methods (Seigneur et al., 2001), the online nesting method uses the same parameters in the
122 global and regional domains, which avoids uncertainties caused by different boundary conditions, and it
123 also provides boundary conditions at higher time resolution (Zhang et al., 2012b; Chen et al., 2015), thus
124 improving the performance of the model at the regional scale.

125 This model includes emission, horizontal and vertical advection (Walcek and Aleksic, 1998),
126 diffusion (Byun and Dennis, 1995), dry deposition (Zhang et al., 2003), gaseous chemistry (CBM-Z,
127 Carbon Bond Mechanism version Z, Zaveri and Peters, 1999), heterogeneous chemistry (Li et al., 2012),
128 aqueous reactions in clouds, and wet scavenging (Stockwell et al., 1990). It has been successfully and
129 widely applied to simulate the spatial-temporal distribution characteristics of gaseous pollutants, aerosol
130 components, and the long-distance transportation of mercury (Chen et al., 2015; Chen et al., 2014; Wei
131 et al., 2019; Ye et al., 2021; Du et al., 2019). In addition, advanced particle microphysics (APM) has been
132 incorporated to simulate new particle formation processes and predict the particle number concentrations
133 at global and regional scales (Chen et al., 2021).

134 **2.2 Development of the PAH module**

135 The PAH processes in the IAP-AACM model include gaseous-phase reaction, heterogeneous
136 reaction, gas-particle partitioning, air-soil exchange, dry deposition, and wet scavenging. The simulated
137 species include BaP, Benzo[b]fluorathene (BbF), Benzo[k]fluorathene (BkF), and Indeno[1,2,3-
138 cd]pyrene (IcdP) in the gas and particulate phases (Wu et al., 2024). In this study, we mainly focus on
139 BaP due to its highly carcinogenic nature and the relatively rich observations.

140 **2.2.1 Gaseous-phase reactions**

141 PAHs are degraded through reactions with various atmospheric oxidants such as hydroxyl radical
142 (OH), nitrate radical (NO₃), and ozone (O₃) in the troposphere (Lammel and Schili, 2007). Among these
143 oxidants, the reactions with OH are considered to be the most important pathway for the removal of
144 PAHs. The nighttime reaction of PAHs with NO₃ is also important in the atmosphere (Keyte et al., 2013).

145 Therefore, reactions of gaseous-phase BaP with OH, NO₃, and O₃ are all considered in the model. The
 146 second-order rate coefficients are 5.0×10⁻¹¹, 5.4×10⁻¹¹, and 2.6×10⁻¹⁷ cm³ molecules⁻¹ s⁻¹, respectively
 147 (Inomata et al., 2013; Finlayson-Pitts and Pitts, 2000; Klöpffer et al., 2007).

148 2.2.2 Heterogeneous reaction

149 In the case of BaP, the heterogeneous reaction with O₃ is considered to be the dominant loss
 150 (Finlayson - Pitts and Pitts, 2000; Efstathiou et al., 2016). Studies have shown that the process of
 151 heterogeneous reaction can be well described by the Langmuir-Hinshelwood mechanism (Kahan et al.,
 152 2006; Kwamena et al., 2007), in which BaP is adsorbed to the surface while the O₃ is in phase equilibrium.
 153 The first-order reaction rate coefficient k (s⁻¹) of the Langmuir-Hinshelwood mechanism is as follows:

$$k = \frac{k_{max}K_{O_3}[O_3]}{1 + K_{O_3}[O_3]} \quad (1)$$

$$\frac{\partial C}{\partial t} = -K_{O_3}[O_3] \quad (2)$$

154 Where k_{max} is the maximum rate coefficient, and the value is 0.060±0.018 s⁻¹. $[O_3]$ is the
 155 concentration of O₃ (mol cm⁻³). K_{O_3} is the O₃ to surface equilibrium constant (0.028±0.014×10⁻¹³ cm³).

156 In addition, we incorporated a more detailed parameterization (ROI-T) developed by Mu et al. (2018)
 157 based on the Langmuir-Hinshelwood mechanism. The scheme emphasizes the importance of
 158 representing the dependence of degradation on temperature and humidity, when coated by organic
 159 aerosols The first-order reaction rate coefficient k (s⁻¹) is given by Eq. (3).

$$k = base + \frac{max - base}{1 + (\frac{xhalf}{[O_3]})^{rate}} \quad (3)$$

160 Where $base$, max , $rate$, and $xhalf$ are all the parameterizations of the heterogeneous reaction,
 161 with specific values shown in Mu et al. (2018). In our study, we coupled these two parameterizations as
 162 two options for O₃ degradation by heterogeneous reaction in IAP-AACM. The model results using these
 163 two schemes were compared to analyze the influence of heterogeneous reaction schemes on BaP
 164 concentration. The ROI-T scheme was used as the default in this study.

165 2.2.3 Gas-particle partitioning

166 The partition of compounds between the gas and particulate phases is parameterized with the gas-
 167 particle partitioning coefficient (K_p , m³ μg⁻¹) (Harner and Bidleman, 1998):

$$K_p = \left(\frac{[PAH]_p}{[TSP]} \right) / [PAH]_g \quad (4)$$

168 Where $[PAH]_g$ and $[PAH]_p$ are the concentrations of PAHs in the gas and particulate phase
 169 ($\mu\text{g m}^{-3}$), and $[TSP]$ is the concentration of total suspended particles (TSP, $\mu\text{g m}^{-3}$) in the atmosphere
 170 ($\mu\text{g m}^{-3}$).

171 Adsorption onto black carbon (BC) and absorption into aerosol organic matter (OM) are two
 172 important mechanisms of gas-particle partitioning (Odabasi et al., 2006). Therefore, we use the gas-
 173 particle partition coefficient equation to represent these two mechanisms, which was derived by Dachs
 174 and Eisenreich, 2000:

$$K_p = \left[\frac{(f_{OM} MW_{OCT} \delta_{OCT}) K_{OA}}{(\rho_{OCT} MW_{OM} \delta_{OM} 10^{12})} \right] + \left[\left(\frac{f_{BC} a_{BC} K_{SA}}{a_{AC} 10^{12}} \right) \right] \quad (5)$$

175 Where MW_{OCT} and MW_{OM} are the mean molecular weights of octanol and OM phase (g mol^{-1}),
 176 δ_{OCT} and δ_{OM} are the activity coefficient of the absorbing compound in octanol and OM phase,
 177 respectively. f_{OM} and f_{BC} are the mass fractions of OM phase on TSP and the BC in the aerosol. ρ_{OCT}
 178 is the density of octanol (0.820 kg L^{-1}). a_{BC} and a_{AC} are the specific surface areas of BC ($62.7 \text{ m}^2 \text{ g}^{-1}$,
 179 Jonker and Koelmans, 2002) and activated carbon (AC), respectively. In this study, we use the same
 180 assumption as Odabasi et al. (2006) ($MW_{OCT}/MW_{OM} = 1$, $\delta_{OCT}/\delta_{OM} = 1$, and $a_{BC}/a_{AC} = 1$).

$$\log K_{OA} = A + B/(T) \quad (6)$$

181 Where K_{OA} is the octanol-air partitioning coefficient (temperature dependent). T is the
 182 temperature (K). The values of A and B are 5382 and -6.5, respectively (Odabasi et al., 2006).

$$\log P_L = m_L(T)^{-1} + b_L \quad (7)$$

$$\log K_{SA} = -0.85 \log P_L + 8.94 - \log \left(\frac{998}{a_{BC}} \right) \quad (8)$$

183 Where P_L is the supercooled liquid vapor pressure (Pa). The values of b_L and m_L are 12.59 and
 184 -5252, respectively (Dachs and Eisenreich, 2000). K_{SA} is the soot-air partitioning coefficient (L kg^{-1}),
 185 which is a function of P_L and a_{BC} (van Noort, 2003).

186 2.2.4 Air-soil exchange

187 The semi-volatility and persistence of PAHs allow them to dynamically exchange between the
 188 atmosphere and soil by deposition and re-volatilization from ground surfaces (Semeena and Lammel,
 189 2005). These processes can affect the distribution and long-distance transport of PAHs in the environment.
 190 As described by Hansen et al. (2004), air-soil exchange is parameterized following Strand and Hov

191 (1996), which is based on Jury et al. (1983). Here, soil (standard soil) is considered to be a homogeneous
 192 layer of thickness $z_s = 0.15$ m, and standard values and chemical properties are provided by Jury et al.
 193 (1983) (Table S1). The differential equation for the change of concentrations in soil and air can be
 194 expressed by Eq. (9) and Eq. (10):

$$\frac{\partial c_s}{\partial t} = \frac{1}{z_s} (F_{exc,soil} + F_{wet}) - k_{soil} c_s \quad (9)$$

$$\frac{\partial c_a}{\partial t} = -\frac{1}{z_a} F_{exc,soil} \quad (10)$$

195 Where C_a and C_s are the concentrations of PAHs in the atmosphere and soil, respectively. The z_a
 196 is the lowest atmospheric layer depths (m), F_{wet} is the wet deposition flux ($\text{mol s}^{-1} \text{m}^{-2}$). k_{soil} is the
 197 degradation rate in soil, which is estimated to be $2.2 \times 10^{-8} \text{ s}^{-1}$ (Finlayson - Pitts and Pitts, 2000; Klöpffer
 198 et al., 2007; Lammel et al., 2009). The air–soil exchange flux ($F_{exc,soil}$) is given by Eq. (11):

$$F_{exc,soil} = K_{a/s} (c_a - \frac{c_s}{K_{soil-air}}) \quad (11)$$

199 $K_{soil-air}$ is the partitioning coefficient between soil and air, which is given by Karickhoff (1981):

$$K_{soil-air} = 4.11 \times 10^{-4} \times \rho_s f_{oc} K_{OA} \quad (12)$$

200 Where f_{oc} is the fraction of OC in soil and 4.11×10^{-4} is a constant with units of $\text{m}^3 \text{kg}^{-1}$. ρ_s is the
 201 density of soil. $K_{a/s}$ is the overall exchange velocity (m s^{-1}), which can be estimated by Eq. (13) (Strand
 202 and Hov, 1996):

$$K_{a/s} = \frac{D_G^{air} a^{10/3} (1-l-a)^{-2} + D_L^{water} l^{10/3} K_{WA} (1-l-a)^{-2}}{z_s/2} \quad (13)$$

203 Where D_G^{air} and D_L^{water} are the air and liquid diffusion coefficient ($\text{m}^2 \text{s}^{-1}$), respectively. K_{WA} is
 204 the water-air partitioning coefficient. The differential equation is solved the ODEPACK
 205 (<https://github.com/jacobwilliams/odepack>).

206 2.2.5 Dry and wet deposition

207 PAHs can be removed from the atmosphere and enter terrestrial ecosystems through dry and wet
 208 deposition (Cao et al., 2021). Dry deposition and wet scavenging have been included in IAP-AACM. For
 209 the gaseous species of PAHs, their wet scavenging is assumed to be the same as xylene in the CBMZ
 210 mechanism, which is also an aromatic hydrocarbon like BaP; for the PAHs in the particle phase, these
 211 two processes are treated similarly to that of organic aerosol.

212 **2.3 Risk assessment**

213 The incremental lifetime cancer risk (ILCR) is widely used to calculate the risk of human exposure
214 to PAHs (Nam et al., 2021). The carcinogenic risk of PAHs to humans through different exposure routes
215 was calculated based on the health risk evaluation model proposed by the U.S. Environmental Protection
216 Agency (EPA) (Smith et al., 1999).

217 The national population data at 1 km×1 km (at the Equator) resolution in 2013 and 2018 were
218 obtained from the LandScan (Oak Ridge National Laboratory; database can be accessed via:
219 <https://landscan.ornl.gov>, last access: 20 January 2024) and re-gridded to 1°× 1° and 0.33°× 0.33° to
220 match the model resolution.

221 **2.3.1 Daily exposure dose**

222 Dermal contact and inhalation are regarded as the major routes of human exposure to BaP (Li et al.,
223 2010; Ma et al., 2020; Zhang et al., 2016). In this study, the health risk for the entire population and three
224 groups (adult women, adult men, and children) are calculated. The daily exposure dose (ADD) to PAHs
225 through the two exposure routes is calculated as follows:

$$ADD_{der} = \frac{C \times SA \times ABS \times AF \times EF \times ED}{AT \times BW} \quad (14)$$

$$ADD_{inh} = \frac{C \times IR \times EF \times ED}{AT \times BW} \quad (15)$$

226 Where ADD_{der} and ADD_{inh} are the average daily exposure dose that enters the body through the
227 dermal contact and inhalation, respectively ($\text{ng kg}^{-1} \text{ day}^{-1}$), C is the concentration of PAHs (ng m^{-3}). IR
228 is the inhalation rate ($\text{m}^3 \text{ d}^{-1}$). AF is the dermal adherence rate ($\text{mg cm}^{-2} \text{ d}^{-1}$). EF and ED are the
229 exposure duration (d a^{-1}) and period (a), respectively. BW is the body weight (kg). SA is the skin
230 exposed surface area (cm^2). ABS is the skin absorption factor. AT is the average exposure time (d).
231 The values are shown in Table S2.

232 **2.3.2. Incremental lifetime cancer risk (ILCR)**

233 The ILCR was calculated based on the ADD:

$$ILCR_{der} = ADD_{der} \times SFO_{der} \times CF \quad (16)$$

$$ILCR_{inh} = ADD_{inh} \times SFO_{inh} \times CF \quad (17)$$

$$TILCR = ILCR_{der} + ILCR_{inh} \quad (18)$$

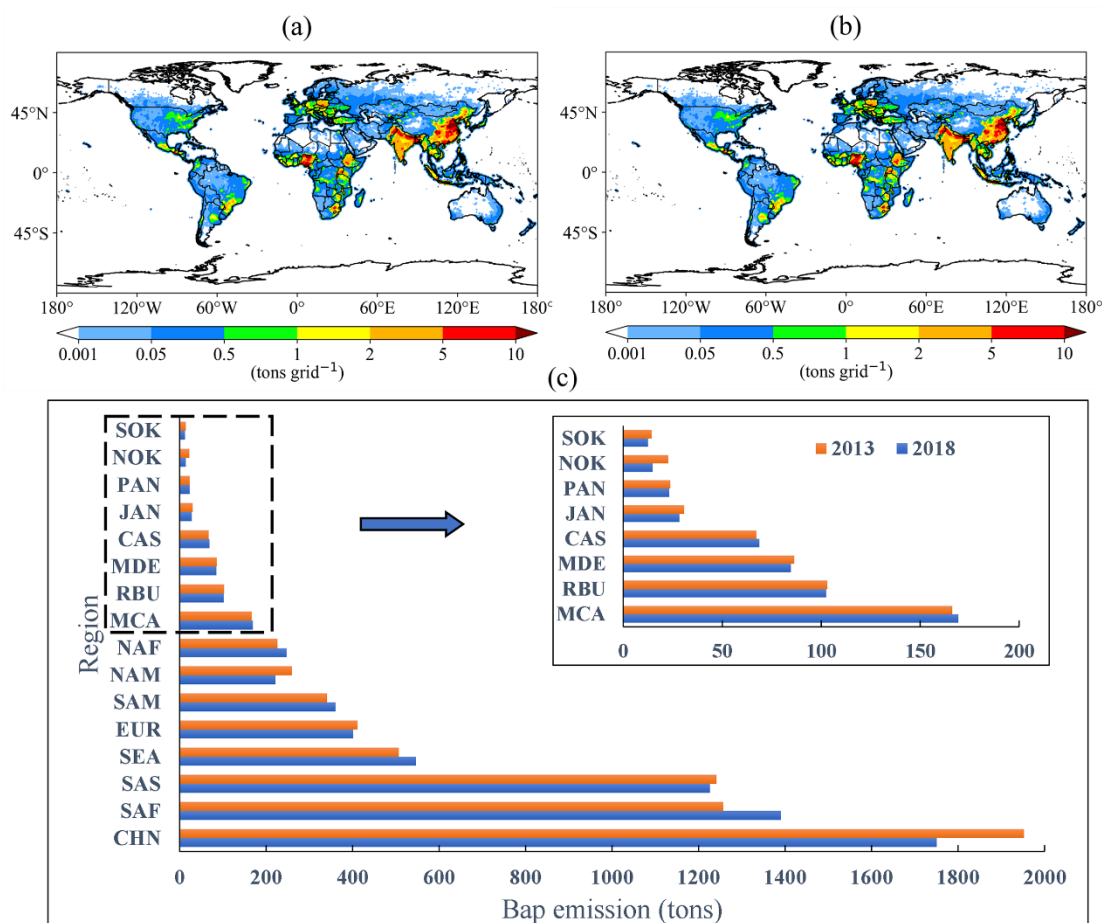
234 Where $ILCR_{der}$ and $ILCR_{inh}$ are lifetime cancer risks through the dermal contact and inhalation,
235 respectively. $TILCR$ is the total lifetime cancer risk of exposure through the two pathways. SFO is a
236 cancer slope factor (kg day mg^{-1}) and CF is the conversion factor. The values are shown in Table S2.
237 For carcinogen, an $ILCR$ less than 1×10^{-6} indicates negligible cancer risk, an $ILCR$ between 1×10^{-6}
238 and 1×10^{-4} indicates potential cancer risk, and an $ILCR$ larger than 1×10^{-4} indicates high potential
239 cancer risk.

240 **3 Experiments setup and observation data**

241 **3.1 Experiments setup**

242 In this study, we used two nested domains covering the whole globe and East Asia as shown in Fig.
243 S1. The horizontal resolutions are $1^\circ \times 1^\circ$ and $0.33^\circ \times 0.33^\circ$, respectively. A total of 20 vertical layers are
244 used in IAP-AACM. The first layer of the model is approximately 50 m deep and the top layer extends
245 to 20 km. The simulation results from January 1st to December 31st 2013 and from January 1st to
246 December 31st 2018 were used for analysis. Each simulation had a one-month spin-up before January 1st
247 to reduce the influence of initial conditions. The global version of the Weather Research and Forecasting
248 model (WRF, version 3.7.1) (Zhang et al., 2012a; Skamarock et al., 2008) provides the meteorological
249 fields to drive the IAP-AACM. The initial and boundary conditions of the global WRF were produced
250 by Final Analysis data (FNL) from the National Centers for Environmental Prediction (NCEP).

251 The emission inventory of BaP in 2013 and 2018 was derived from the Emissions Database for
252 Global Atmospheric Research (EDGAR, Crippa et al., 2020, available from
253 https://edgar.jrc.ec.europa.eu/dataset_pop60#sources, last access: 15 December 2023). We mainly
254 analyzed the results using EDGAR emission, which mainly includes anthropogenic sources such as
255 power, transportation, industrial, agricultural, and energy for buildings. An additional simulation for 2013
256 using the emission inventory developed by the research group of Peking University (PKU)
257 (<http://inventory.pku.edu.cn>, last access: 10 February 2023) was used to investigate the uncertainties
258 from emissions. The resolution of both emission inventories is $0.1^\circ \times 0.1^\circ$. Therefore, we re-gridded the
259 emissions inventories to match the model grids at $1^\circ \times 1^\circ$ and $0.33^\circ \times 0.33^\circ$ resolution.



260
 261 **Figure 1. Spatial distributions of total emissions of BaP in (a) 2013 and (b) 2018 based on the EDGAR**
 262 **inventory. (c) BaP emissions for 16 regions (except oceans, Arctic, and Antarctic) in 2013 and 2018.**

263 The global total emissions of BaP in 2013 and 2018 are shown in Fig. 1a and 1b, respectively. The
 264 annual emissions in different regions (Fig. S1) were also calculated (Fig. 1c). The global emissions of
 265 BaP were 7,166.9 t in 2013 and 7,109.5 t in 2018, respectively. Figure. S3 shows emissions and changes
 266 for different sectors in China, Africa, South Asia, Europe, North America, and South America in 2013
 267 and 2018, where residential, industry, and agriculture are the main sources of BaP. China is one of the
 268 largest BaP-emitting countries in the world. Its emissions were 1,952.2 t in 2013 and 1,750.2 t in 2018,
 269 respectively, accounting for about 27.2% and 24.6% of the world, which are generally consistent with
 270 the results of Shen et al. (2013) (20.3%). The residential sector is the largest emission source of BaP in
 271 China, accounting for 63.2% of the total emissions, followed by industrial sector (35.6%) in 2013. Africa
 272 and South Asia had the second and third-largest emissions, with residential combustion accounting for
 273 87.3% and 84.0% of total emissions, respectively. This is related to the widespread use of biomass fuels
 274 for heating and cooking in developing countries (Shen et al., 2013). Emissions from China, Southern

275 Africa, and South Asia accounted for 62.1% and 61.4% of the world. China, Australia, South Asia,
276 Europe, North America, South Korea, Japan, and North Korea displayed a declining trend from 2013 to
277 2018. China experienced the largest decline (10.4%), due to the active emission control measures taken
278 under the “Air Pollution Prevention and Control Action Plan” implemented in 2013. The industrial sector
279 contributed the most to the decline of BaP emissions, followed by the residential combustion, which
280 decreased by 18.9% and 5.1% from 2013 to 2018, respectively, which are mainly related to the
281 strengthened industrial emission standards, upgraded industrial boilers, and the development of clean
282 fuels. The above results are generally consistent with the conclusions of Wang et al. (2021) in which
283 PAHs emissions decreased by 11.36% from 2013 to 2017, with the industrial and residential sectors
284 decreasing by 17.32% and 10.58%, respectively. The emissions increased in Africa (10.3%) and South
285 America (5.9%), mainly caused by the emission increase in residential (10.6%) and agricultural (9.5%)
286 sectors, respectively.

287 To understand the change in BaP concentrations, we conducted five experiments: the first and
288 second experiments simulated the BaP concentration using the emissions in 2013 and 2018 driven by the
289 corresponding meteorological fields. The third experiment used the emission in 2018 but kept the
290 meteorological conditions in 2013 to investigate the effects of meteorological condition changes on the
291 concentration of BaP. Studies neglecting the heterogeneous loss of BaP and using two different
292 heterogeneous schemes were also performed to explore the impacts of heterogeneous reactions on BaP
293 concentrations in the fourth and fifth experiments

294 **3.2 Observational data**

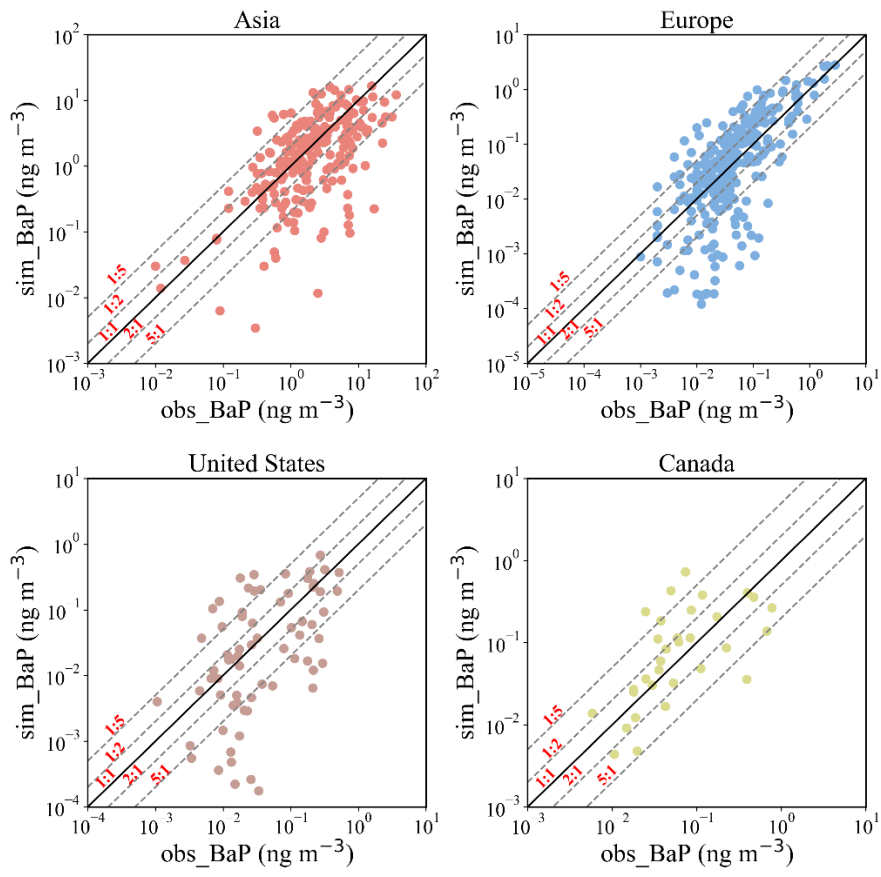
295 To evaluate the model performance, we collected the PAHs observation from several available
296 datasets and more than 50 published papers. The observational data are summarized as follows: (1)
297 European Monitoring and Evaluation Program (EMEP, available from
298 <https://projects.nilu.no/ccc/reports.html>, last access: 15 December 2023): this includes annual and
299 monthly averages of BaP concentrations at 36 European sites in Spain, Finland, France, Germany,
300 Norway, Poland, and other countries in Europe; (2) National Air Pollution Surveillance network: (NAPS,
301 <https://data-donnees.az.ec.gc.ca/data/air/monitor/>: last access: 30 January 2024): this includes daily
302 averages (autumn and winter) of BaP concentrations at Canadian stations; (3) Integrated Atmospheric
303 Deposition Network: (IADN, <https://iadnviz.iu.edu/datasets/index.html>, last access: 20 January 2023):

304 this includes monthly mean concentrations of BaP at 6 sites in the United States and Canada from 1990
305 to 2021; (4) Chinese Persistent Organic Pollutants (POPs) Soil and Air Monitoring Program Phase II
306 (SAMP-II, Ma et al., 2018): this is carried out by the International Joint Research Center for Persistent
307 Toxic Substances (IJRC-PTS), focusing on 11 urban centers in China (Beijing, Xi'an, Nanchang,
308 Kunming, Lanzhou, Chengdu, Harbin, Dalian, Lhasa, Guangzhou, and Shihezi), 1 suburb and 3
309 background/rural areas. This observational data only covers the period from August 2008 to July 2010;
310 (5) observational data collected from published papers (these sources are listed in supplementary material)
311 (Wu et al., 2024).

312 PAHs measurements data are very sparse compared to conventional pollutants (e.g., PM_{2.5}). Since
313 most of the data are not continuous in time, we selected data covering at least 10 days in years as close
314 as possible to the simulation year (2013) and used the mean values for comparison. The comparison of
315 the monthly variation was conducted only for sites in Europe where observations were continuous and
316 available. The locations of the BaP observation sites are shown in Fig. S2. The site information is listed
317 in Table S5 and Table S6.

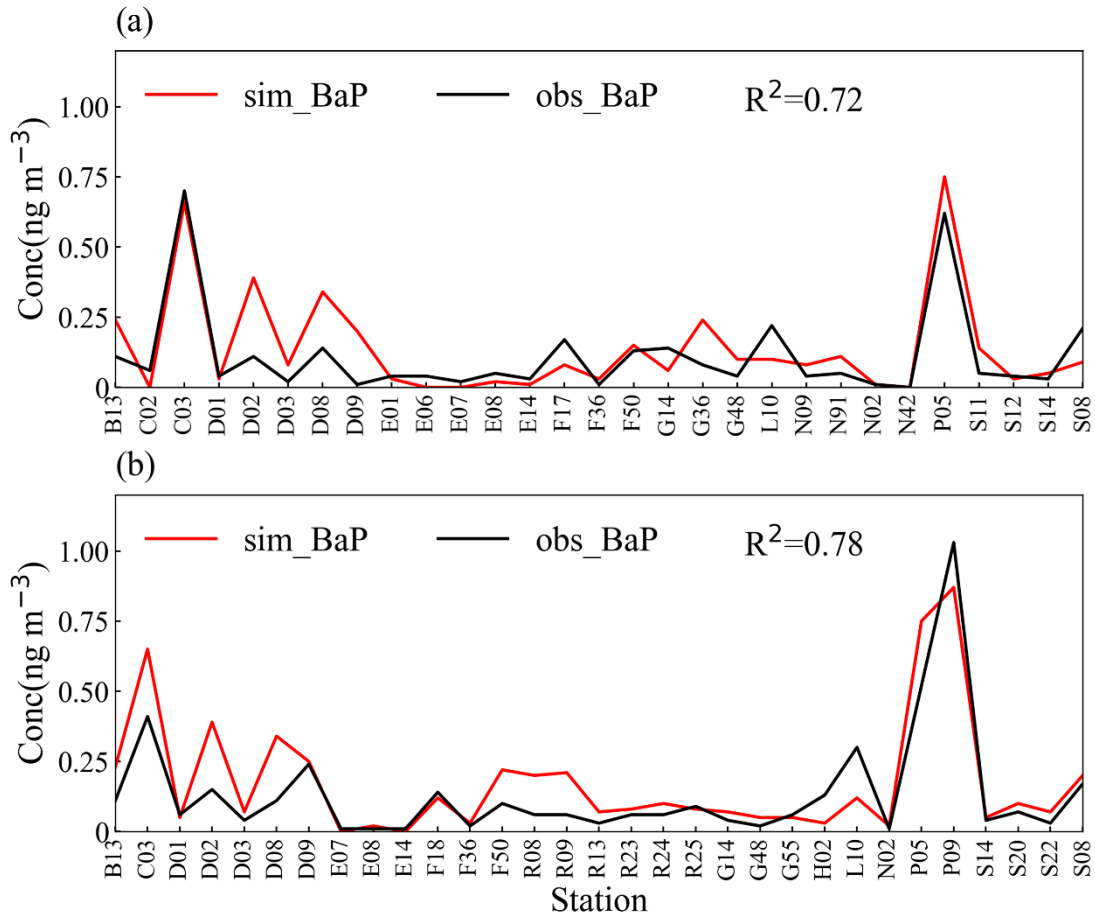
318 **4 Results**

319 **4.1 Global distribution of BaP and health risks**



320
 321
 322
 323

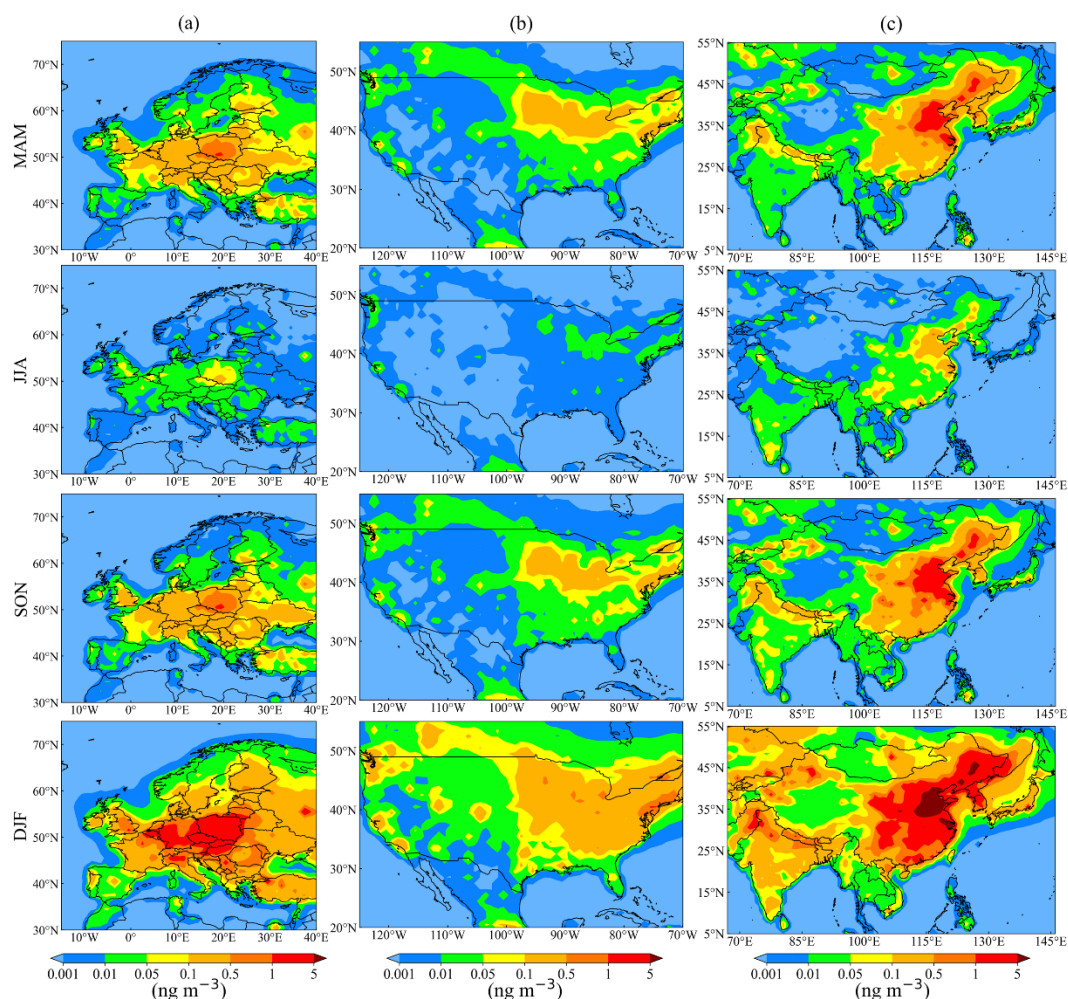
Figure 2. Comparison of simulated (sim_BaP) and observed (obs_BaP) annual mean concentrations of BaP in Asia (pink), Europe (blue), United States (brown), and Canada (green) in 2013. The solid black line shows a ratio of 1 : 1 and the dashed gray lines show ratios of 5 : 1, 2 : 1, 1 : 2, and 1 : 5.



324
325
326

Figure 3. Comparison of the BaP annual mean simulated (red) concentrations with observed (black) values at European sites in (a) 2013 and (b) 2018.

327 To evaluate the performance of the IAP-AACM model, annual mean simulated concentrations in
328 Asia, Europe, the United States, and Canada were compared with observations (Fig. 2). The results show
329 that the model can reproduce nearly half of the observation samples within a factor of 2 and most
330 observations within a factor of 5 at sites in Asia, Europe, the United States, and Canada. The number of
331 sites where BaP was underestimated was greater than the number where it was overestimated due to the
332 averaging effect of subgrid emissions. Considering that some of the comparisons are not in the same year,
333 a certain discrepancy between the model and observation is expected. Further, a specific comparison was
334 performed using the data from about 30 stations in Europe (Fig. 3a and b). High concentrations were
335 mainly found in polluted areas of Central Europe, consistent with the simulation of Gusev et al. (2017),
336 such as Poland (P05) and the Czech Republic (C03) with observed values of 0.70 and 0.62 ng m⁻³,
337 respectively, and simulated concentrations of 0.66 and 0.75 ng m⁻³ in 2013, The model successfully
338 reproduced the observed concentrations and differences between sites.

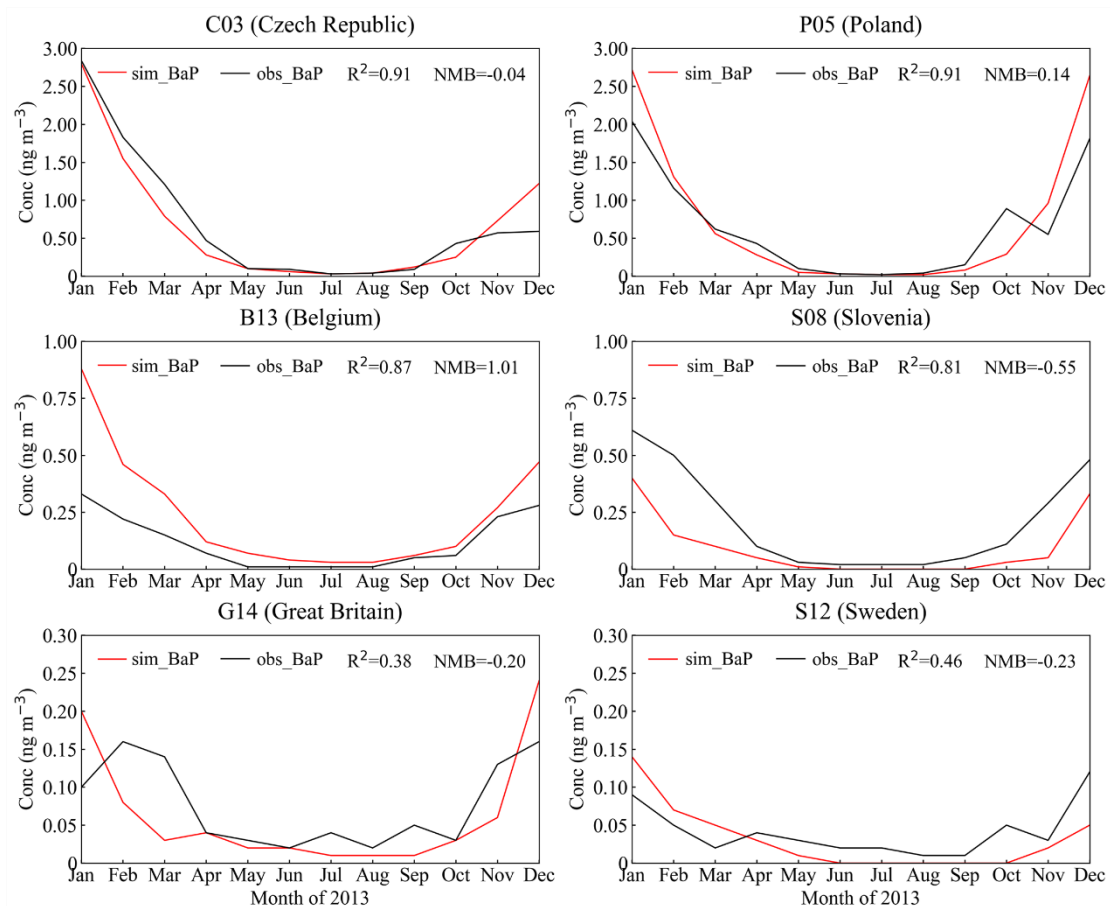


339
340
341

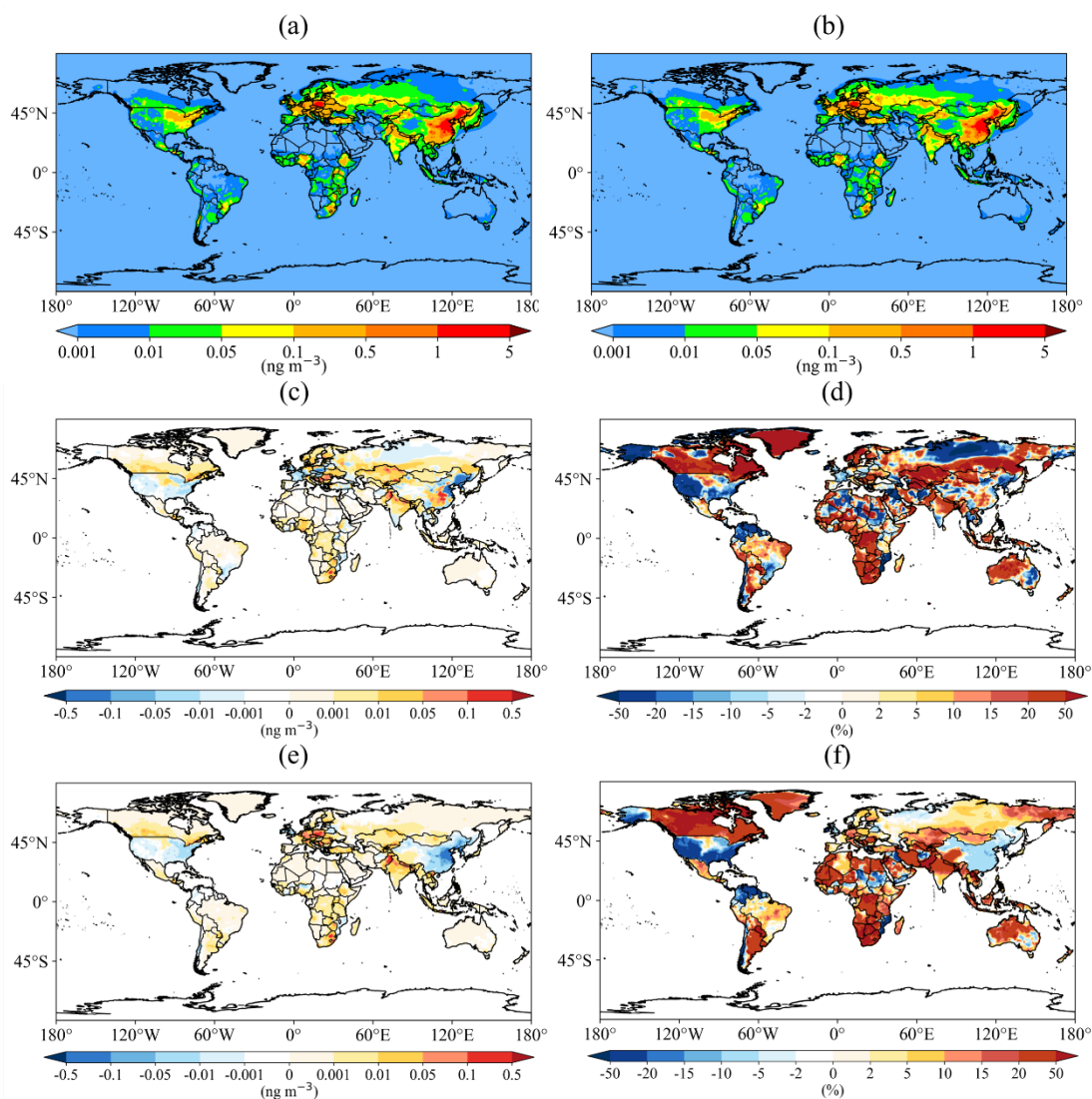
Figure 4. Spatial distributions of seasonal mean concentrations in (a) Europe, (b) the contiguous United States, and (c) East Asia in 2013.

342 Figure 4 shows the seasonal mean concentrations of BaP in Europe, the contiguous United States,
343 and East Asia in four seasons: March–April–May (MAM, representing spring), June–July–August (JJA,
344 representing summer), September–October–November (SON, representing autumn), and December–
345 January–February (DJF, representing winter). Generally, BaP had the highest concentration in winter and
346 lowest in summer. This is caused by the larger emission and poorer atmospheric diffusion conditions in
347 winter than in summer. In the contiguous United States, the concentrations were lower than 1 ng m^{-3} in
348 all four seasons, consistent with the simulation of Galarneau et al. (2014). In east China, large areas have
349 a concentration of $> 1 \text{ ng m}^{-3}$ and even $> 5 \text{ ng m}^{-3}$ in BTH in winter. Europe shows a distribution of
350 high values in central areas and low values in remote areas. In Central Europe (such as Poland and the
351 Czech Republic), large areas have concentrations between $1\text{--}5 \text{ ng m}^{-3}$ in winter. High concentrations
352 were also reported by Bieser et al. (2012). The observation clearly shows higher concentrations at sites
353 in Poland and the Czech Republic than at other sites in Europe (Fig. 5). The model successfully

354 reproduces the seasonal variation of BaP at sites in Europe. The simulation had a good agreement with
 355 observations at C03 and P05 with correlation coefficient (R^2) of 0.91 and 0.91, and normalized mean
 356 bias (NMB) of -0.04 and 0.14, respectively. The R^2 was higher than 0.8 at B13 and S08, and the NMB
 357 was 1.01 and -0.55. In summary, IAP-AACM can reasonably simulate the spatial distribution and
 358 seasonal variation of BaP.



359
 360 **Figure 5. Comparison of the BaP month mean simulated concentrations (red) with observed values (black)**
 361 **at six stations in Europe in 2013.**

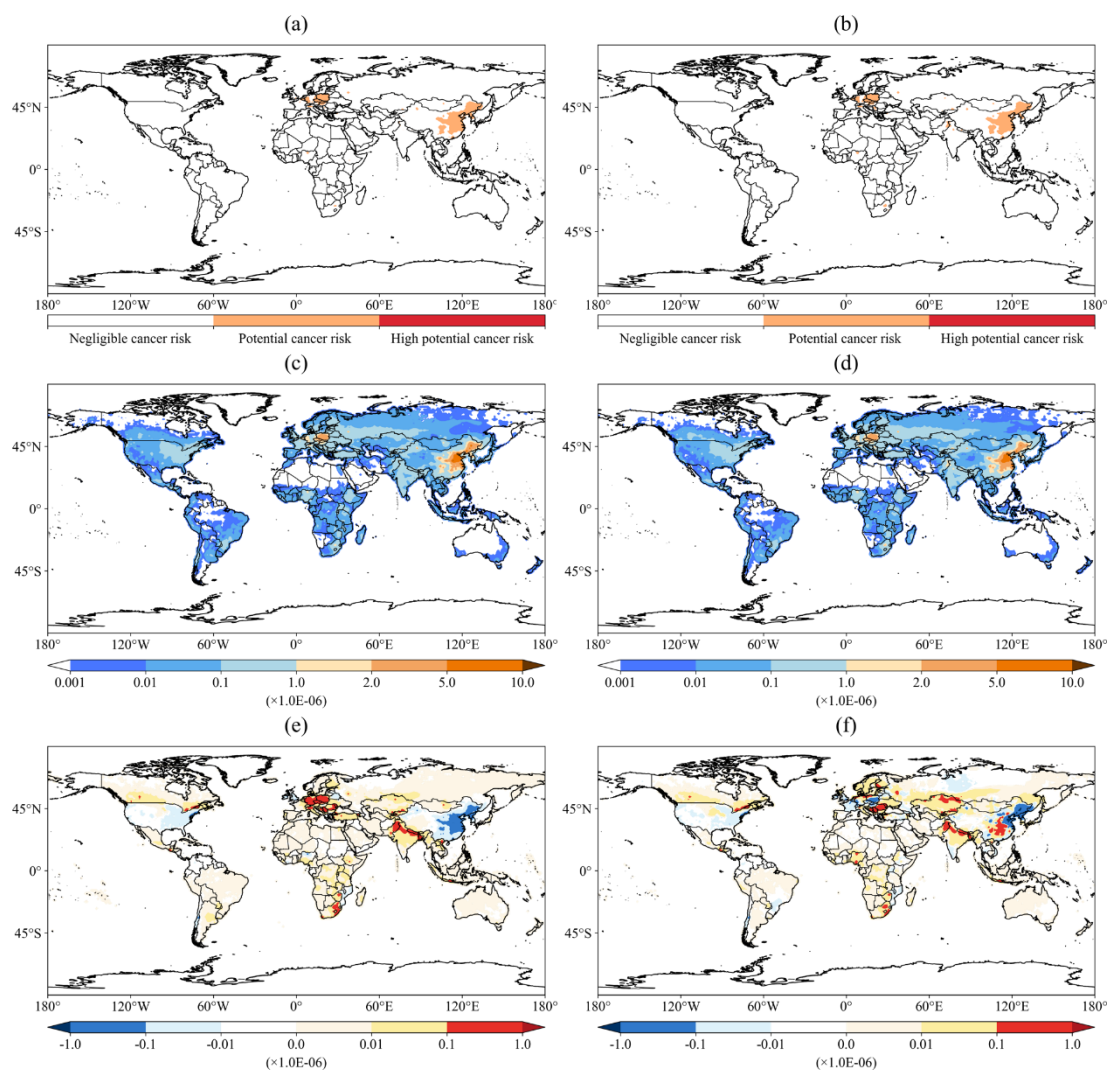


362

363 **Figure 6. Spatial distributions of annual mean BaP concentrations based on the EDGAR in (a) 2013 and (b)**
 364 **2018 . The (c/e) absolute and (d/f) relative concentration changes from 2013 to 2018 are shown considering**
 365 **(c, d) both emissions and meteorological conditions or (e, f) only emissions, respectively.**

366 The spatial distribution of annual mean BaP concentrations based on the EDGAR inventory in 2013
 367 and 2018 are shown in Fig. 6a and b. The spatial distribution of BaP concentrations in 2018 was similar
 368 to that in 2013. The spatial pattern was consistent with the emission distribution in the EDGAR inventory.
 369 High concentrations of BaP were found in northern and eastern China, and central Europe, even
 370 exceeding the European Union target value for BaP (1 ng m⁻³), indicating an urgent need to control BaP
 371 and other PAHs. The absolute and relative concentration changes from 2013 to 2018 are shown in Fig.
 372 6c and d. The most significant decreases were seen in Russia, the United States, eastern and northern
 373 China. By contrast, the concentration in India, Europe, Southeast Asia, and South Africa shows an
 374 increase, with the average annual concentration increasing by 19.4%, 1.2%, 11.2%, and 18.3%,

375 respectively. When only considering the impact of emission change (Fig. 6e and f), the decrease in the
 376 eastern United States is larger and the increase in central Europe is larger. In particular, there is an obvious
 377 decline (about 8.0%) across China, which demonstrates the effect of the emission reduction measures.
 378 These results clearly show the large influence of meteorological changes. It is crucial to consider
 379 meteorological factors when evaluating emission changes and reduction measures through monitoring
 380 concentrations in the atmosphere.



381
 382 **Figure 7. The distribution of health risks grade in (a) 2013 and (b) 2018, the distribution of TILCR in (c)**
 383 **2013 and (d) 2018, and the absolute from 2013 to 2018 when considering the change in (e) emissions only, (f)**
 384 **both emissions and meteorological conditions.**

385 The global distribution of health risks grade and TILCR (the sum of ILCR values of the two
 386 exposure routes after averaging the parameters of the different groups) in 2013 and 2018 are shown in
 387 Fig. 7. It can be seen that most of the countries just face negligible cancer risk, and no regions facing
 388 high potential cancer risk when evaluation is based on annual mean concentration. However, eastern

389 China and central Europe are in potential cancer risk, with the highest TILCR values of 1.54×10^{-5} (1.47
390 $\times 10^{-5}$) and 4.62×10^{-6} (4.23×10^{-6}) in 2013 (2018), respectively. It should be noted that in other
391 developing countries such as Africa, India, and Southeast Asia, TILCR values increased in 2018
392 compared to 2013, with the highest (mean) values increasing from 1.47×10^{-6} (4.15×10^{-8}) to 2.26×10^{-6}
393 (4.78×10^{-8}), from 1.41×10^{-6} (2.03×10^{-7}) to 1.73×10^{-6} (2.43×10^{-7}), and from 8.02×10^{-7} (6.07×10^{-8}) to
394 1.14×10^{-6} (6.75×10^{-8}), respectively. These countries will be likely to face potential even high potential
395 cancer risks, especially in winter. In addition, Lou et al. (2023) has indicated that health risks in South
396 Asia and Africa will increase in the future with the increase of residential fuels use along with the
397 population growth in these regions. It is clear that clean development is a necessary consideration for
398 developing countries to avoid the health risks posed by PAHs.

399 **4.2 Distribution of PAHs and their change in China**

400 Figure 8 shows the annual mean distribution of BaP in China in 2013. The concentrations ranged
401 from 0.02 to 6.14 ng m⁻³. Overall, high concentrations were simulated in the North China Plain, East
402 China, and Northeast China, significantly higher than in Northwest and Southwest China, consistent with
403 previous studies (Ma et al., 2020; Yan et al., 2019). This can be largely attributed to the industrial and
404 residential coal combustion in these regions. Among the different provinces in China, there are 14
405 provinces with concentrations higher than the ambient air quality standards of China (1 ng m⁻³, GB 3095–
406 2012: <http://www.zhb.gov.cn/>, last access: 6 April 2014). Shanghai had the highest concentration of 6.14
407 ng m⁻³, followed by Tianjin (4.56 ng m⁻³), Beijing (3.41 ng m⁻³), and Shandong (3.10 ng m⁻³). The
408 concentrations in the Northwest and Southwest regions were lower, with Tibet having the lowest
409 concentration of only 0.02 ng m⁻³. This is due to lower levels of industrial activities and population
410 density in these regions compared to eastern regions. In addition, the high topography of northwest
411 regions has good air circulation and is conducive to the diffusion and dilution of atmospheric pollutants.
412 In 2013, Beijing had the highest BaP concentration in winter (14.03 ng m⁻³), possibly due to the high
413 population density, high number of vehicles, and frequent industrial activities in Beijing. Moreover,
414 Beijing lies on the North China Plain, where the meteorological conditions make it easier for air
415 pollutants to stay and accumulate, resulting in a high concentration of BaP.

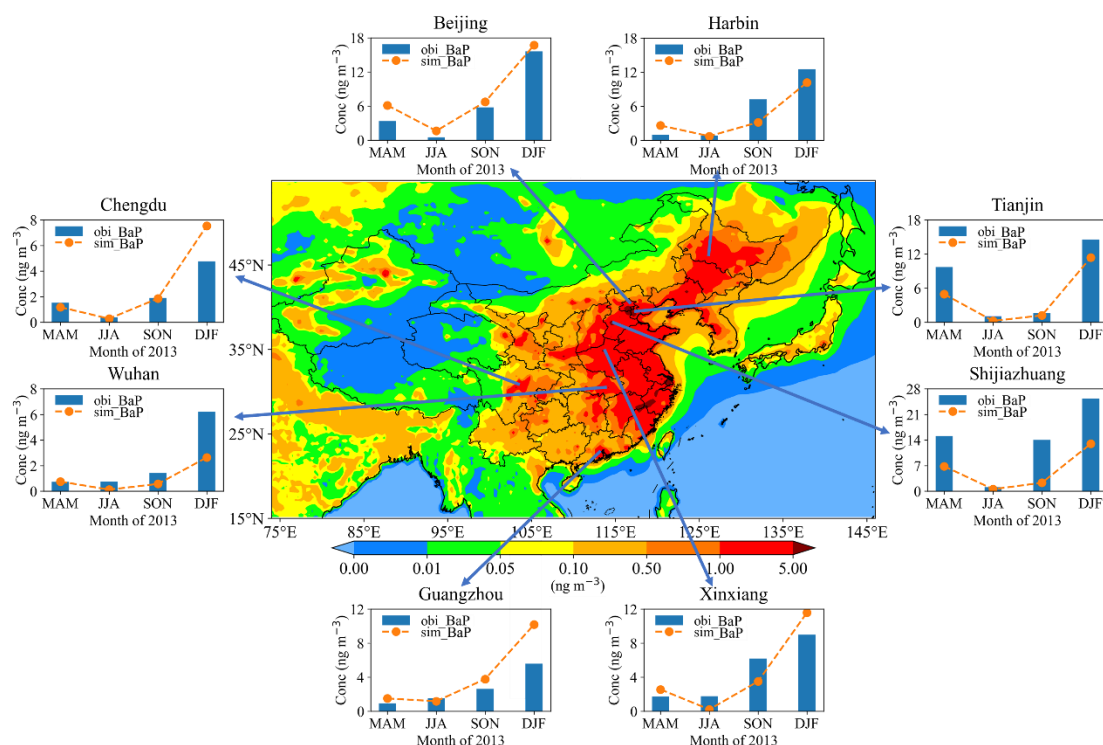


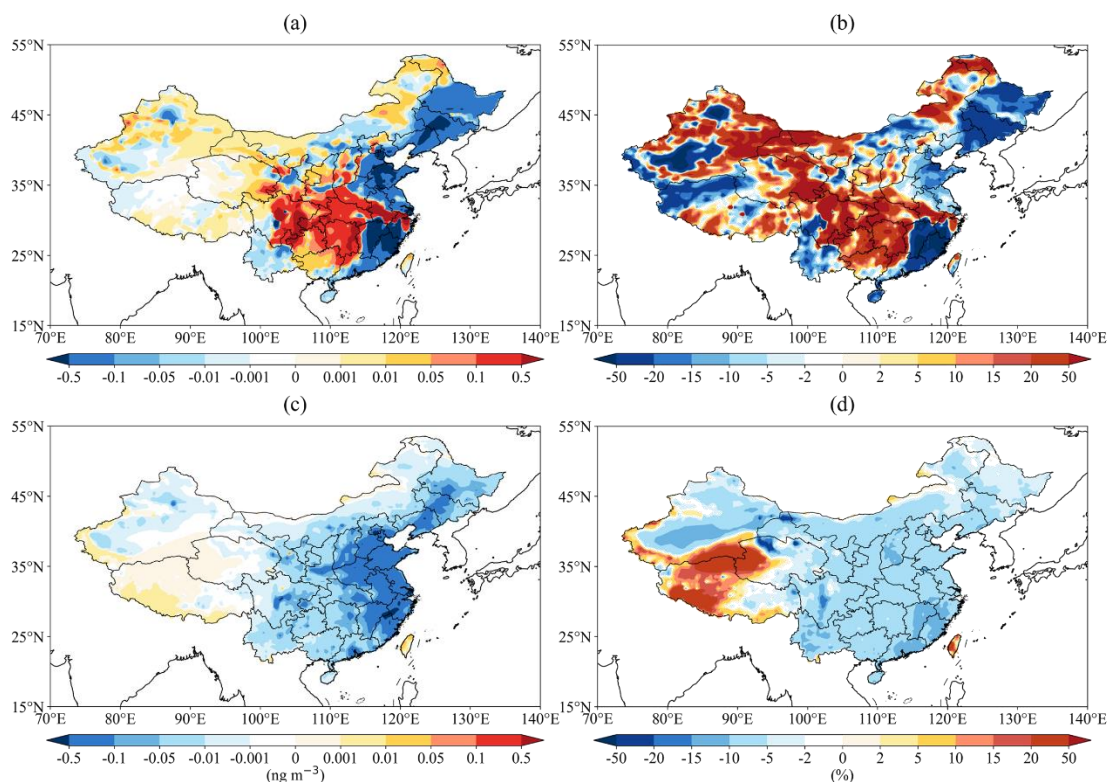
Figure 8. Spatial distributions of annual mean concentrations in China. Comparison of the BaP month mean simulated concentrations (orange) with observed values (blue) at eight cities in 2013.

416
417
418

419 To reveal the seasonal variation of BaP concentrations in key regions, we analyzed the concentration
420 in eight major cities, i.e., Beijing, Tianjin, Shijiazhuang, Xinxiang, Wuhan, Chengdu, Guangzhou, and
421 Harbin (seen in Fig. 8). It can be seen that the seasonal variations of BaP in these cities are similar, with
422 the highest values in winter and the lowest in summer. The seasonal difference in northern cities was
423 significantly greater than that in southern cities. In Beijing, Xinxiang, Tianjin, Harbin, and Shijiazhuang,
424 the differences in concentration between winter and summer were as high as 15.06, 11.76, 11.14, 9.45,
425 and 12.42 ng m^{-3} , respectively. This is caused by the fact that coal-fired heating is very common in
426 northern China, which can significantly increase the PAH emissions in winter (Yan et al., 2019). In
427 addition, the meteorological conditions also affect the seasonal variation of PAHs, as the lower
428 temperature, less rainfall, and weaker solar radiation during the winter support the formation of a stable
429 inversion layer, greatly limiting the diffusion of BaP in the air (Lin et al., 2015; Quan et al., 2014).

430 By comparing the simulated concentrations with the observed concentrations, we find that the model
431 can capture the BaP concentrations and the seasonal pattern in different cities. For example, the observed
432 and simulated concentrations show good consistency in the spring, summer, and autumn of Chengdu and
433 in the summer, autumn, and winter of Beijing, with a deviation of only 0.04 to 1.1 ng m^{-3} . However, there
434 were some deviations between the simulated and observed concentrations. The most obvious

435 underestimation is seen in Shijiazhuang. This is probably due to the underestimation of emissions and
 436 the model resolution that may not fully resolve the pollution in cities with urban areas smaller than the
 437 model grid. The model performance could be improved by using more precise emissions and increasing
 438 grid resolution. Nonetheless, the model can capture the magnitude and seasonal variation in BaP
 439 concentration well in China and in other countries around the world, and can therefore be used to evaluate
 440 the health effects of BaP exposure.

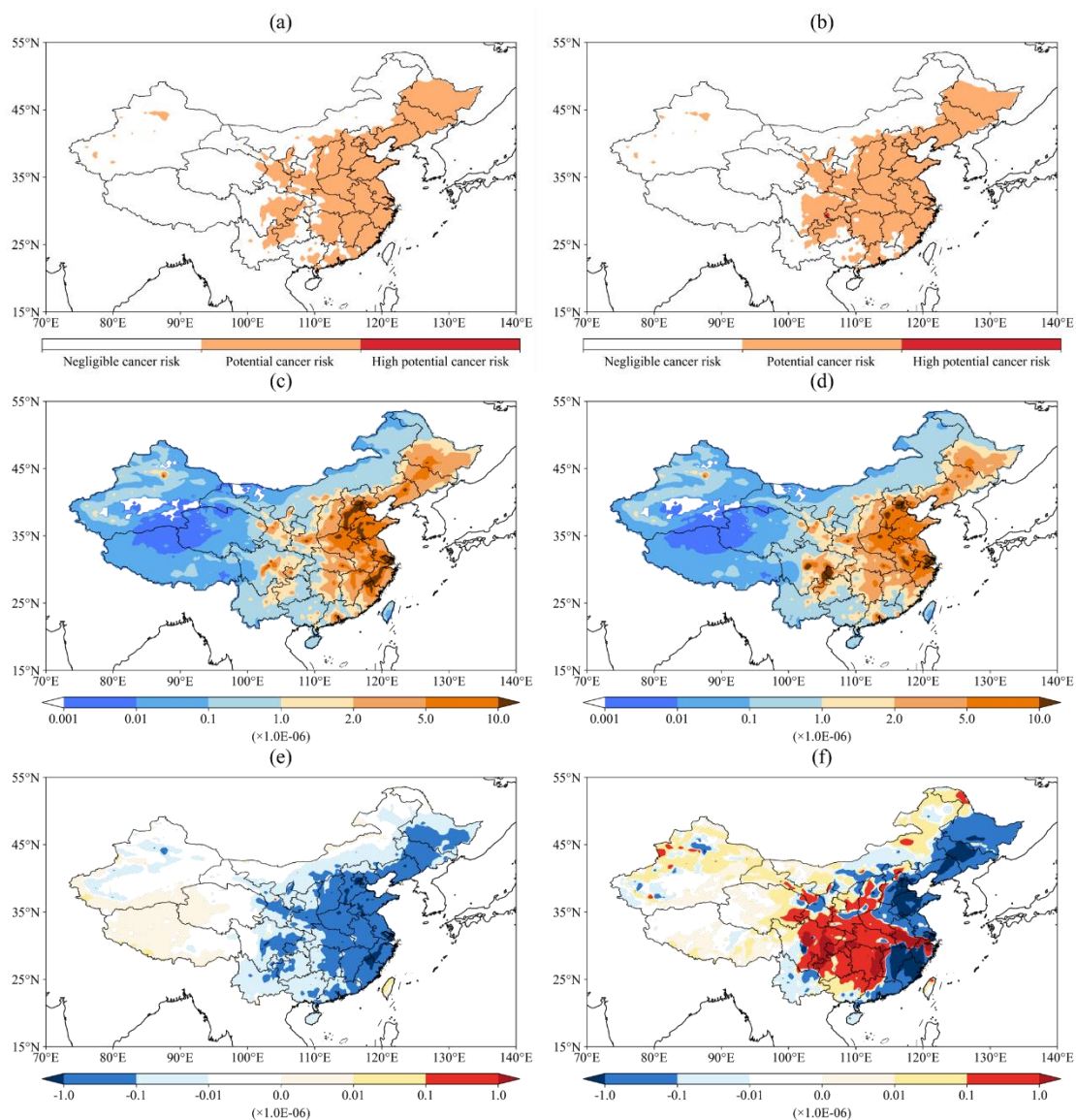


441
 442 **Figure 9. The (a/c) absolute and (b/d) relative concentration changes from 2013 to 2018 in mean annual BaP**
 443 **concentrations in China are shown considering (a, b) both emissions and meteorological conditions or (c, d)**
 444 **only emissions, respectively.**

445 The changes from 2013 to 2018 are shown in Fig. 9. The trend and magnitude of changes differ
 446 greatly across different regions. The largest decrease ($> 20\%$) was seen in northeastern and southeastern
 447 China, consistent with the other studies in Beijing (Lin et al., 2024), Shanghai (Yang et al., 2021),
 448 Shenyang (Zhang et al., 2023), Tianjin (Zhang et al., 2022). The concentration also decreased in the
 449 North China Plain, benefitting from the emission reduction policies such as the development of cleaner
 450 energy sources and the control of industrial emissions. The concentration decrease was larger than the
 451 emission reduction over these areas. By contrast, as shown in Fig. 9a, the concentration in the Sichuan
 452 Basin showed an inverse trend although the emission decreased. This phenomenon demonstrates the

453 large impact of unfavorable meteorological conditions with decreasing temperatures and planetary
454 boundary layer height compared to 2013 (Ding et al., 2019). When only considering the emissions
455 changes, the concentration shows a decrease over most regions consistent with the emission change. It
456 should be noted that the decrease in BaP in the two experiments is significantly lower than that of PM_{2.5}.
457 As shown in Fig. 9b (Fig. 9d), the BaP concentration decreased by 9.1% and 6.7% (8.5% and 9.4%) in
458 the BTH and the YRD, respectively. Wang et al. (2019) showed that compared with 2013, the
459 concentration of PM_{2.5} in the BTH, the YRD, and the PRD in 2017 decreased by 39.6%, 34.3%, and
460 27.7%, respectively. For cities in North and East China, the concentration still exceeds the national limit
461 value (1 ng m⁻³) although the concentration of BaP decreased significantly in 2018. For example, the BaP
462 concentrations in Shanghai, Beijing, and Tianjin considering changes in both emissions and meteorology
463 were 5.32, 3.31, and 3.38 ng m⁻³, respectively, and those with emission changes alone were 5.58, 3.11,
464 and 4.17 ng m⁻³, indicating that the concentrations are mainly affected by the emission sources. The
465 results in the central and western cities differed greatly between the two experiments, especially in
466 Chongqing, Sichuan, and Guizhou, indicating that changes were mainly related to meteorological
467 conditions. Therefore, when formulating emission reduction policies, it is necessary to take into account
468 the effects of changes in meteorological conditions as well as emission sources.

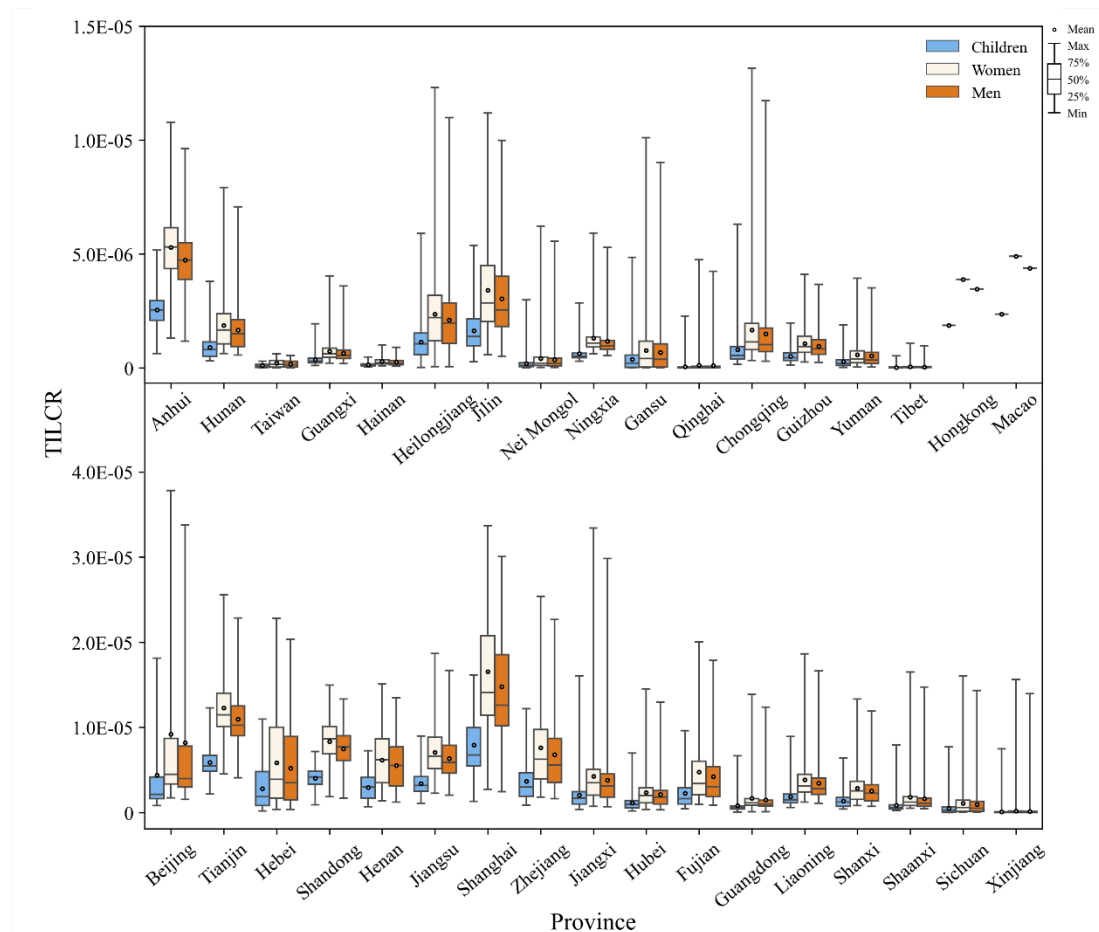
469 **4.3 Health risks of PAHs in China**



470
 471 **Figure 10. The distribution of health risks grade in China in (a) 2013 and (b) 2018, the distribution of**
 472 **TILCR in (c) 2013 and (d) 2018, and the TILCR changes from 2013 to 2018 when considering the change in**
 473 **(e) emissions only, (f) both emissions and meteorological conditions.**

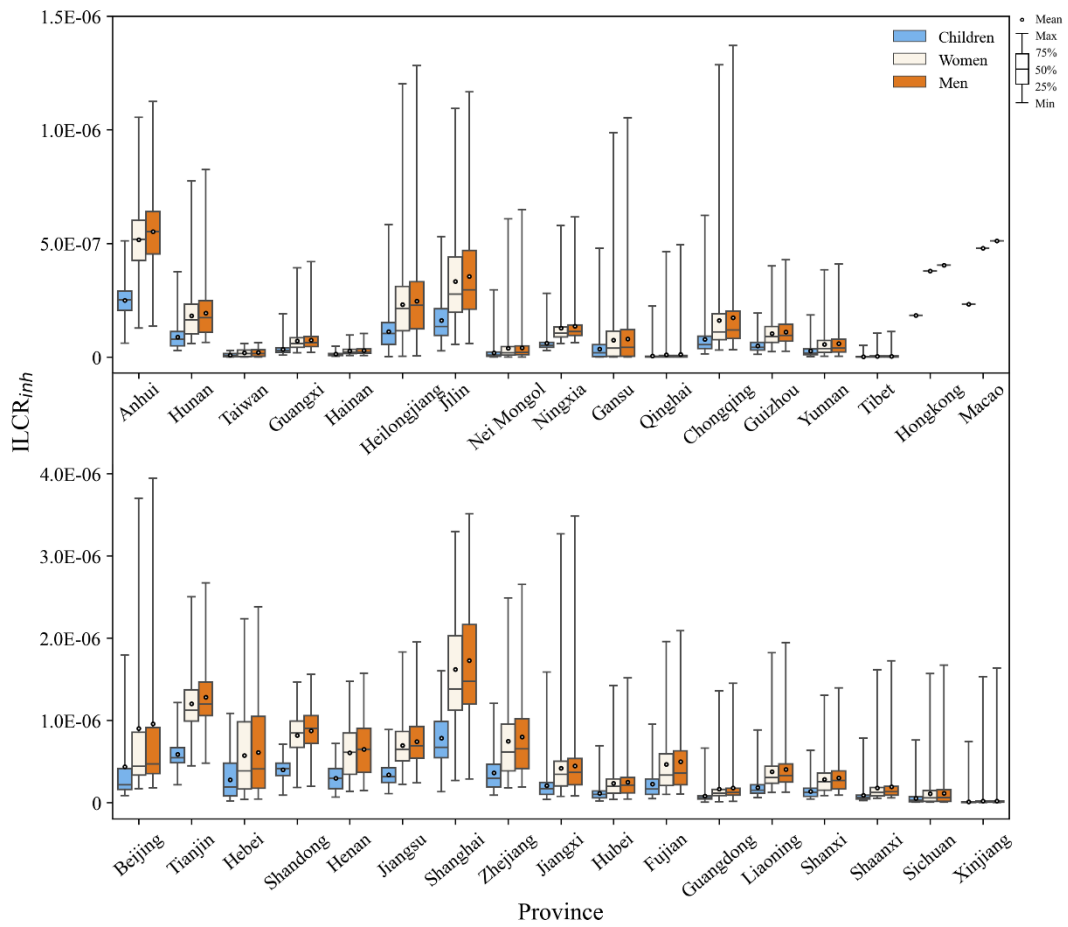
474 In this section, the health risks of BaP are assessed based on the simulation over the nested domain
 475 (domain 2) covering China. As shown in Fig. 10a and b, the health risks in western China is negligible,
 476 while there is a potential cancer risk in eastern China. Figure 9c and d show the TILCR values in 2013
 477 and 2018, and Fig. 10e and f show the change from 2013 to 2018 when only emissions or both emissions
 478 and meteorological conditions are considered. It can be seen that the spatial distribution of TILCR (Fig.
 479 10c) is consistent with the spatial distribution of the BaP annual concentrations (Fig. 6), showing higher
 480 risk in eastern regions than in the western regions (Han et al., 2020). The values of the TILCR in China
 481 ranged from 3.0×10^{-9} to 3.5×10^{-5} , with an average value of 1.4×10^{-6} . Compared with 2013, the average

482 TILCR in 2018 decreased by 8.0×10^{-8} , which is mainly directly related to the decrease in concentration.
 483 From the perspective of two exposure routes, $ILCR_{inh}$ and $ILCR_{der}$ values ranged from 2.8×10^{-10} – 3.3×10^{-6}
 484 6 and 2.7×10^{-9} – 3.2×10^{-5} , with an average value of 1.3×10^{-2} and 1.3×10^{-6} , respectively. The values of
 485 $ILCR_{der}$ were one order of magnitude higher than the $ILCR_{inh}$.



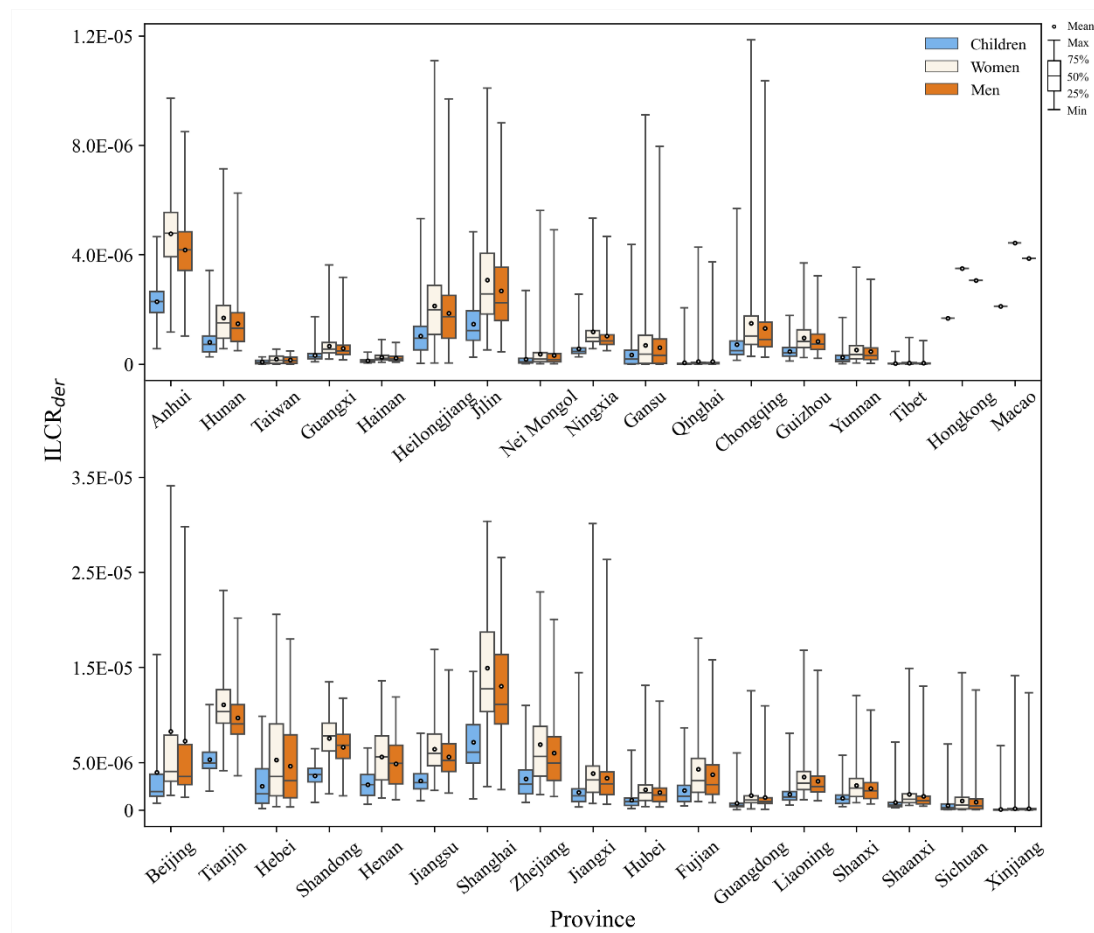
486
 487 **Figure 11. The TILCR values for the three age groups (Children, Women, and Men) in different provinces**
 488 **of China in 2013.**

489 The TILCR values of the three groups in 2013 and 2018 calculated using Eq. (14)-Eq. (18) are
 490 shown in Fig. 11 and Fig. S4, respectively, which ranged from 1.55×10^{-9} to 3.78×10^{-5} (1.60×10^{-9} to
 491 3.41×10^{-5}). The order of TILCR was women (1.46×10^{-6}) > men (1.31×10^{-6}) > children (7.03×10^{-7}), which
 492 was similar to that of dermal contact exposure. Overall, 29.2% of TILCR were higher than 1.0×10^{-6} , and
 493 1.2% of TILCR were higher than 1.0×10^{-5} in 2013. There was a slight decrease in TILCR values in 2018
 494 due to the lower concentrations of BaP, with 27.9% and 0.7% of TILCR higher than 1.0×10^{-6} and 1.0×10^{-5} ,
 495 respectively. There is no high cancer risk in China, but there are potential cancer risks in some areas,
 496 which should be paid attention to.



497
 498
 499

Figure 12. The ILCR_{inh} values for the three age groups (Children, Women, and Men) in different provinces of China in 2013.



500
501
502

Figure 13. The ILCR_{der} values for the three age groups (Children, Women, and Men) in different provinces of China in 2013.

503
504
505
506
507
508
509
510
511
512

The ILCR values of the three groups in China through inhalation and dermal exposure routes are shown in Fig. 12 and Fig. 13, and the ILCR in 2018 are shown in Fig. S5 and Fig. S6. For the inhalation pathway, the average ILCR_{inh} was 1.22×10^{-7} ($< 1.0 \times 10^{-6}$). The order of ILCR_{inh} was men (1.53×10^{-7}) > women (1.43×10^{-7}) > children (6.95×10^{-8}), and the risk for men was about twice that of children, but was lower in women than in men. This may be caused by the fact that the inhalation and metabolic rate of women are weaker than men (Bai et al., 2020). The highest average value was found in Shanghai, where the average ILCR_{ing} for the three groups were 1.72×10^{-6} , 1.62×10^{-6} , and 7.84×10^{-7} , respectively. Han et al. (2020) found cases of excess cancer due to exposure to PAHs in large cities such as Shanghai. Only 1.6% of the three groups had ILCR_{ing} higher than 1×10^{-6} , indicating that the health risks from inhalation exposure were low. A similar conclusion was mentioned in an earlier review (Yan et al., 2019).

513
514

For dermal contact exposure, the average ILCR_{der} was 1.04×10^{-6} ($> 1.0 \times 10^{-6}$). Compared to the ILCR_{inh}, the health risk to adults was slightly higher than that to children, but women had higher risk

515 values than men. This may be caused by the fact that the body weight of women is weaker than men. The
516 order of $ILCR_{der}$ was women (1.32×10^{-6}) > men (1.15×10^{-6}) > children (6.33×10^{-6}), which is similar to
517 the results of previous studies (Bai et al., 2020). Among the three groups, 27.4% of the $ILCR_{der}$ values
518 were higher than 1×10^{-6} , and 0.7% were higher than 1×10^{-5} . This shows that there is a greater potential
519 carcinogenic risk through dermal contact exposure.

520 **5 Discussion**

521 It should be noted that model results have some uncertainties even though our model simulated the
522 main features of PAHs concentrations reasonably well. Firstly, we simulated lower BaP concentrations
523 when using the PKU inventory than when using the EDGAR inventory over most continental areas,
524 except for Inner Mongolia, eastern Russia, and north China (Fig. S7). The difference can be as high as
525 0.5 ng m^{-3} over some areas in wintertime although the spatial and temporal distributions are consistent.
526 The emission inventory remains to be constrained by more observations. Current observations are too
527 sparse to conduct detailed evaluation in areas where long-term measurements are not available. Secondly,
528 we tested the influence of heterogeneous reaction schemes on simulation. When heterogeneous reactions
529 were not considered, the model significantly overestimated the concentration of BaP (Fig. S8), suggesting
530 the importance of heterogeneous loss of BaP. Using the Langmuir-Hinshelwood mechanism, we
531 simulated lower concentrations in most regions of the northern hemisphere, especially in winter (Fig.
532 S9). However, the difference between the simulated results of the two mechanisms is significantly
533 reduced in summer due to high temperature and high humidity. This is consistent with the results by Mu
534 et al. (2018), i.e., low temperature and low humidity can significantly increase the lifetime of BaP.
535 Comparison of model results using different schemes and model intercomparison would further help
536 identify the uncertainties and improve model performance.

537 **6 Conclusion**

538 In this study, the PAHs modules were coupled into the IAP-AACM model to investigate the global
539 and regional distribution of PAHs. The model has the state-of-the-art heterogeneous mechanism and
540 allows us to consistently examine the multi-scale distribution of PAHs. Comparison with observations
541 shows that the model can reproduce the different concentrations of BaP at the stations in Asia, Europe,

542 the United States, and Canada. The model can capture the seasonal variation of BaP, with lower
543 concentrations in summer and higher concentrations in winter over the continents in the northern
544 hemisphere. The global distributions of BaP in 2013 and 2018 were very similar, with high concentrations
545 concentrated in eastern China and central Europe, even exceeding EU limits (1 ng m^{-3}). Compared with
546 2013, BaP concentration in 2018 showed a decrease in the United States, Poland, France, Czech, and
547 some regions in China. By contrast, the concentrations increased by $>10\%$ in India and South Africa.
548 Populations in these regions are facing increased health risks posed by PAHs.

549 In China, the decline in BTH (8.5%) and YRD (9.4%) benefitted from “the Action Plan”. However,
550 the decline was significantly less than that of conventional pollutants, such as $\text{PM}_{2.5}$. Changes in
551 meteorological conditions had a significant influence on changes in BaP concentration, which increased
552 in the Sichuan Basin and central China even though the emissions over these areas decreased due to the
553 control measures. There was a slight decrease in total ILCR (TILCR) values in 2018 compared to 2013.
554 For the different exposure routes, the dermal contact was an order of magnitude higher than the inhalation
555 route. The TILCR for adults was greater than that for children. 29.2% of TILCR were higher than 1.0×10^{-6} ,
556 indicating that there are still potential cancer risks in China. More attention must be paid to the non-
557 traditional pollutant pollutants and strict but different control measures are necessary to reduce PAHs'
558 concentration and health risks. Especially in the fall and winter seasons, the concentration of BaP and
559 the associated health risk is significantly higher than in other seasons. Management efforts on key sectors
560 (e.g., industrial and residential sources) should be further strengthened. In heavily polluted cities, using
561 clean energy to replace coal combustion, adjusting the energy structure of factory production, and
562 developing innovative technologies with lower and even no emissions would be helpful to reduce PAHs
563 pollution.

564 In summary, our study developed an effective tool for simulating the global and regional
565 concentrations of BaP and other PAHs and quantified the health risks in China from 2013 to 2018. Model
566 analysis indicated that emission inventories and heterogeneous reactions can significantly affect the
567 simulated BaP concentrations. Accurate emissions and reasonable representation of heterogeneous
568 reactions would greatly reduce the gap between model results and observation. However, the current
569 observations are insufficient to fully evaluate and constrain the model. Especially, long-term observations
570 are needed in Asia, India, and Africa. These regions are still facing significant health risks. In addition,

571 monitoring in the background and remote regions (such as the Arctic) is necessary to quantify the long-
572 range transport of PAHs.

573

574 *Code and data availability.* The source code and their introduction of IAP-AACM can be found online
575 via Zenodo (<https://doi.org/10.5281/zenodo.12214119>). The simulated data can be found via Zenodo
576 (<https://doi.org/10.5281/zenodo.11595165>). All the observational data are provided in the supplement
577 and can be found via Zenodo (<https://doi.org/10.5281/zenodo.11595165>).

578

579 *Author contributions.* ZcW developed the model, prepared the input data, performed the simulations and
580 analysis, and wrote the paper with suggestions from all co-authors. XC supported the coding and
581 conceived the idea of the paper. XC and ZfW revised the paper and provided scientific guidance through
582 all research advances. JL, ZW, LW, HC, YL, MQ, XT, and QW modified the manuscript. WW supported
583 the emission data. YW, ZZ, and ZJ supported the data analysis. All listed authors have read and approved
584 the final manuscript.

585

586 *Competing interests.* The authors declare that they have no conflict of interest.

587

588 *Disclaimer.* Publisher's note: Copernicus Publications remains neutral about jurisdictional claims in
589 published maps and institutional affiliations.

590

591 *Acknowledgements.* We are particularly grateful to Prof. Oliver Wild at Lancaster University for his help
592 with improving the paper. We thank Prof. Alexey Gusev at EMEP for providing MSC-E results as a good
593 reference to test our model performance. We also thank the National Key Scientific and Technological
594 Infrastructure project "Earth System Science Numerical Simulator Facility" (EarthLab).

595

596 *Financial support.* This research has been supported by the National Key R&D Program of China (Grant
597 NO.2020YFA0607801), the National Natural Science Foundation of China (Grant NO. 42377105) and
598 the National Key Scientific and Technological Infrastructure project "Earth System Science Numerical
599 Simulator Facility".

600 **References**

- 601 Aulinger, A., Matthias, V., Quante, M.: CMAQ simulations of the benzo(a)pyrene distribution over
602 Europe for 2000 and 2001, *Atmospheric Environment*, 43, 4078-4086,
603 <https://doi.org/10.1016/j.atmosenv.2009.04.058>, 2009.
- 604 Aulinger, A., Quante, M., Matthias, V.: Introducing a Partitioning Mechanism for PAHs into the
605 Community Multiscale Air Quality Modeling System and Its Application to Simulating the
606 Transport of Benzo(a)pyrene over Europe, *Journal of Applied Meteorology and Climatology*,
607 46, 1718-1730, <https://doi.org/10.1175/2007jamc1395.1>, 2007.
- 608 Baek, S. O., Field, R. A., Goldstone, M. E., Kirk, P. W., Lester, J. N., Perry, R.: A review of atmospheric
609 polycyclic aromatic-hydrocarbons-sources, fate and behavior, *Water Air and Soil Pollution*, 60,
610 279-300, <https://doi.org/10.1007/bf00282628>, 1991.
- 611 Bai, L., Chen, W. Y., He, Z. J., Sun, S. Y., Qin, J.: Pollution characteristics, sources and health risk
612 assessment of polycyclic aromatic hydrocarbons in PM_{2.5} in an office building in northern
613 areas, China, *Sustainable Cities and Society*, 53, 10, <https://doi.org/10.1016/j.scs.2019.101891>,
614 2020.
- 615 Bieser, J., Aulinger, A., Matthias, V., Quante, M.: Impact of Emission Reductions between 1980 and 2020
616 on Atmospheric Benzo (a) pyrene Concentrations over Europe, *Water Air and Soil Pollution*,
617 223, 1393-1414, <https://doi.org/10.1007/s11270-011-0953-z>, 2012.
- 618 Byun, D., Schere, K. L.: Review of the governing equations, computational algorithms, and other
619 components of the models-3 Community Multiscale Air Quality (CMAQ) modeling system,
620 *Applied Mechanics Reviews*, 59, 51-77, <https://doi.org/10.1115/1.2128636>, 2006.
- 621 Byun, D. W., Dennis, R.: DESIGN ARTIFACTS IN EULERIAN AIR-QUALITY MODELS -
622 EVALUATION OF THE EFFECTS OF LAYER THICKNESS AND VERTICAL PROFILE
623 CORRECTION ON SURFACE OZONE CONCENTRATIONS, *Atmospheric Environment*, 29,
624 105-126, [https://doi.org/10.1016/1352-2310\(94\)00225-a](https://doi.org/10.1016/1352-2310(94)00225-a), 1995.
- 625 Cao, X. H., Huo, S. L., Zhang, H. X., Zheng, J. Q., He, Z. S., Ma, C. Z., Song, S.: Source emissions and
626 climate change impacts on the multimedia transport and fate of persistent organic pollutants,
627 Chaohu watershed, eastern China, *Journal of Environmental Sciences*, 109, 15-25,
628 <https://doi.org/10.1016/j.jes.2021.02.028>, 2021.

629 Chen, H. S., Wang, Z. F., Li, J., Tang, X., Ge, B. Z., Wu, X. L., Wild, O., Carmichael, G. R.: GNAQPMS-
630 Hg v1.0, a global nested atmospheric mercury transport model: model description, evaluation
631 and application to trans-boundary transport of Chinese anthropogenic emissions, *Geoscientific*
632 *Model Development*, 8, 2857-2876, <https://doi.org/10.5194/gmd-8-2857-2015>, 2015.

633 Chen, S. C., Liao, C. M.: Health risk assessment on human exposed to environmental polycyclic aromatic
634 hydrocarbons pollution sources, *Science of the Total Environment*, 366, 112-123,
635 <https://doi.org/10.1016/j.scitotenv.2005.08.047>, 2006.

636 Chen, X. S., Wang, Z. F., Li, J., Yu, F. Q.: Development of a Regional Chemical Transport Model with
637 Size-Resolved Aerosol Microphysics and Its Application on Aerosol Number Concentration
638 Simulation over China, *Sola*, 10, 83-87, <https://doi.org/10.2151/sola.2014-017>, 2014.

639 Chen, X. S., Yu, F. Q., Yang, W. Y., Sun, Y. L., Chen, H. S., Du, W., Zhao, J., Wei, Y., Wei, L. F., Du, H.
640 Y., Wang, Z., Wu, Q. Z., Li, J., An, J. L., Wang, Z. F.: Global-regional nested simulation of
641 particle number concentration by combing microphysical processes with an evolving organic
642 aerosol module, *Atmospheric Chemistry and Physics*, 21, 9343-9366,
643 <https://doi.org/10.5194/acp-21-9343-2021>, 2021.

644 Crippa, M., Solazzo, E., Huang, G. L., Guizzardi, D., Koffi, E., Muntean, M., Schieberle, C., Friedrich,
645 R., Janssens-Maenhout, G.: High resolution temporal profiles in the Emissions Database for
646 Global Atmospheric Research, *Scientific Data*, 7, 17, [https://doi.org/10.1038/s41597-020-0462-](https://doi.org/10.1038/s41597-020-0462-2)
647 [2](https://doi.org/10.1038/s41597-020-0462-2), 2020.

648 Dachs, J., Eisenreich, S. J.: Adsorption onto aerosol soot carbon dominates gas-particle partitioning of
649 polycyclic aromatic hydrocarbons, *Environmental Science & Technology*, 34, 3690-3697,
650 <https://doi.org/10.1021/es991201+>, 2000.

651 **Ding, D., Xing, J., Wang, S.X., Liu, K.Y., Hao, J.M.: Estimated Contributions of Emissions**
652 **Controls, Meteorological Factors, Population Growth, and Changes in Baseline Mortality**
653 **to Reductions in Ambient PM_{2.5} and PM_{2.5}-Related Mortality in China, 2013-2017.**
654 ***Environmental Health Perspectives*, 127, 12, <https://doi.org/10.1289/ehp4157>, 2019.**

655 Dong, Z. S., Kong, Z. H., Dong, Z., Shang, L. Q., Zhang, R. Q., Xu, R. X., Li, X.: Air pollution prevention
656 in central China: Effects on particulate-bound PAHs from 2010 to 2018, *Journal of*
657 *Environmental Management*, 344, 11, <https://doi.org/10.1016/j.jenvman.2023.118555>, 2023.

658 Du, H. Y., Li, J., Chen, X. S., Wang, Z. F., Sun, Y. L., Fu, P. Q., Li, J. J., Gao, J., Wei, Y.: Modeling of
659 aerosol property evolution during winter haze episodes over a megacity cluster in northern
660 China: roles of regional transport and heterogeneous reactions of SO₂,
661 Atmospheric Chemistry and Physics, 19, 9351-9370, <https://doi.org/10.5194/acp-19-9351-2019>,
662 2019.

663 Efstathiou, C. I., Matejovičová, J., Bieser, J., Lammel, G.: Evaluation of gas-particle partitioning in a
664 regional air quality model for organic pollutants, Atmospheric Chemistry and Physics, 16,
665 15327-15345, <https://doi.org/10.5194/acp-16-15327-2016>, 2016.

666 Feng, Y. Y., Ning, M., Lei, Y., Sun, Y. M., Liu, W., Wang, J. N.: Defending blue sky in China:
667 Effectiveness of the "Air Pollution Prevention and Control Action Plan" on air quality
668 improvements from 2013 to 2017, Journal of Environmental Management, 252, 13,
669 <https://doi.org/10.1016/j.jenvman.2019.109603>, 2019.

670 Finlayson-Pitts, B. J., Pitts, J. N. Chemistry of the Upper and Lower Atmosphere: Theory, Experiments,
671 and Applications. 2000.

672 Friedman, C. L., Pierce, J. R., Selin, N. E.: Assessing the Influence of Secondary Organic versus Primary
673 Carbonaceous Aerosols on Long-Range Atmospheric Polycyclic Aromatic Hydrocarbon
674 Transport, Environmental Science & Technology, 48, 3293-3302,
675 <https://doi.org/10.1021/es405219r>, 2014.

676 Friedman, C. L., Selin, N. E.: Long-Range Atmospheric Transport of Polycyclic Aromatic Hydrocarbons:
677 A Global 3-D Model Analysis Including Evaluation of Arctic Sources, Environmental Science
678 & Technology, 46, 9501-9510, <https://doi.org/10.1021/es301904d>, 2012.

679 Galarneau, E., Makar, P. A., Zheng, Q., Narayan, J., Zhang, J., Moran, M. D., Bari, M. A., Pathela, S.,
680 Chen, A., Chlumsky, R.: PAH concentrations simulated with the AURAMS-PAH chemical
681 transport model over Canada and the USA, Atmospheric Chemistry and Physics, 14, 4065-4077,
682 <https://doi.org/10.5194/acp-14-4065-2014>, 2014.

683 Gusev, A., Ilyin, I., Rozovskaya, O., Shatalov, V., Travnikov, O., Strijkina I. Assessment of transboundary
684 pollution by toxic substances: Heavy metals and POPs, Meteorological Synthesizing Centre -
685 East, Russia, 74 pp., 2019.

686 Han, F. L., Guo, H., Hu, J. L., Zhang, J., Ying, Q., Zhang, H. L.: Sources and health risks of ambient

687 polycyclic aromatic hydrocarbons in China, *Science of the Total Environment*, 698, 13,
688 <https://doi.org/10.1016/j.scitotenv.2019.134229>, 2020.

689 Hansen, K. M., Christensen, J. H., Brandt, J., Frohn, L. M., Geels, C.: Modelling atmospheric transport
690 of α -hexachlorocyclohexane in the Northern Hemisphere with a 3-D dynamical model: DEHM-
691 POP, *Atmos. Chem. Phys.*, 4, 1125-1137, <https://doi.org/10.5194/acp-4-1125-2004>, 2004.

692 Haritash, A. K., Kaushik, C. P.: Biodegradation aspects of Polycyclic Aromatic Hydrocarbons (PAHs): A
693 review, *Journal of Hazardous Materials*, 169, 1-15,
694 <https://doi.org/10.1016/j.jhazmat.2009.03.137>, 2009.

695 Harner, T., Bidleman, T. F.: Octanol-air partition coefficient for describing particle/gas partitioning of
696 aromatic compounds in urban air, *Environmental Science & Technology*, 32, 1494-1502,
697 <https://doi.org/10.1021/es970890r>, 1998.

698 Inomata, Y., Kajino, M., Sato, K., Ohara, T., Kurokawa, J., Ueda, H., Tang, N., Hayakawa, K., Ohizumi,
699 T., Akimoto, H.: Source contribution analysis of surface particulate polycyclic aromatic
700 hydrocarbon concentrations in northeastern Asia by source-receptor relationships,
701 *Environmental Pollution*, 182, 324-334, <https://doi.org/10.1016/j.envpol.2013.07.020>, 2013.

702 Inomata, Y., Kajino, M., Sato, K., Ohara, T., Kurokawa, J. I., Ueda, H., Tang, N., Hayakawa, K., Ohizumi,
703 T., Akimoto, H.: Emission and Atmospheric Transport of Particulate PAHs in Northeast Asia,
704 *Environmental Science & Technology*, 46, 4941-4949, <https://doi.org/10.1021/es300391w>,
705 2012.

706 Jonker, M. T. O., Koelmans, A. A.: Sorption of polycyclic aromatic hydrocarbons and polychlorinated
707 biphenyls to soot and soot-like materials in the aqueous environment mechanistic considerations,
708 *Environmental Science & Technology*, 36, 3725-3734, <https://doi.org/10.1021/es020019x>, 2002.

709 Jury, W. A., Spencer, W. F., Farmer, W. J.: Behavior Assessment Model for Trace Organics in Soil: I.
710 Model Description, *Journal of Environmental Quality*, 12, 558-564,
711 <https://doi.org/10.2134/jeq1983.00472425001200040025x>, 1983.

712 Kahan, T. F., Kwamena, N. O. A., Donaldson, D. J.: Heterogeneous ozonation kinetics of polycyclic
713 aromatic hydrocarbons on organic films, *Atmospheric Environment*, 40, 3448-3459,
714 <https://doi.org/10.1016/j.atmosenv.2006.02.004>, 2006.

715 Karickhoff, S. W.: Semi-empirical estimation of sorption of hydrophobic pollutants on natural sediments

716 and soils, *Chemosphere*, 10, 833-846, [https://doi.org/10.1016/0045-6535\(81\)90083-7](https://doi.org/10.1016/0045-6535(81)90083-7), 1981.

717 Keyte, I. J., Harrison, R. M., Lammel, G.: Chemical reactivity and long-range transport potential of
718 polycyclic aromatic hydrocarbons - a review, *Chemical Society Reviews*, 42, 9333-9391,
719 <https://doi.org/10.1039/c3cs60147a>, 2013.

720 Klöpffer, W., Wagner, B., Scheringer, M.: Atmospheric degradation of organic substances data for
721 persistence and long-range transport potential, *Environmental Science and Pollution Research*
722 - International, 14, 143-144, <https://doi.org/10.1065/espr2007.04.408>, 2007.

723 Kwamena, N. O. A., Clarke, J. P., Kahan, T. F., Diamond, M. L., Donaldson, D. J.: Assessing the
724 importance of heterogeneous reactions of polycyclic aromatic hydrocarbons in the urban
725 atmosphere using the Multimedia Urban Model, *Atmospheric Environment*, 41, 37-50,
726 <https://doi.org/10.1016/j.atmosenv.2006.08.016>, 2007.

727 Lammel, G., Dvorská, A., Klánová, J., Kohoutek, J., Kukacka, P., Prokes, R., Sehili, A. M.: Long-range
728 Atmospheric Transport of Polycyclic Aromatic Hydrocarbons is Worldwide Problem - Results
729 from Measurements at Remote Sites and Modelling, *Acta Chimica Slovenica*, 62, 729-735, 2015.

730 Lammel, G., Sehili, A. M.: Global fate and distribution of polycyclic aromatic hydrocarbons emitted from
731 Europe and Russia, *Atmospheric Environment*, 41, 8301-8315,
732 <https://doi.org/10.1016/j.atmosenv.2007.06.050>, 2007.

733 Lammel, G., Sehili, A. M., Bond, T. C., Feichter, J., Grassl, H.: Gas/particle partitioning and global
734 distribution of polycyclic aromatic hydrocarbons--a modelling approach, *Chemosphere*, 76, 98-
735 106, <https://doi.org/10.1016/j.chemosphere.2009.02.017>, 2009.

736 Li, J., Wang, Z. F., Zhuang, G., Luo, G., Sun, Y., Wang, Q.: Mixing of Asian mineral dust with
737 anthropogenic pollutants over East Asia: a model case study of a super-duststorm in March 2010,
738 *Atmospheric Chemistry and Physics*, 12, 7591-7607, <https://doi.org/10.5194/acp-12-7591-2012>,
739 2012.

740 Li, R. F., Zhang, J., Krebs, P.: Global trade drives transboundary transfer of the health impacts of
741 polycyclic aromatic hydrocarbon emissions, *Communications Earth & Environment*, 3, 13,
742 <https://doi.org/10.1038/s43247-022-00500-y>, 2022.

743 Li, Z., Mulholland, J. A., Romanoff, L. C., Pittman, E. N., Trinidad, D. A., Lewin, M. D., Sjödin, A.:
744 Assessment of non-occupational exposure to polycyclic aromatic hydrocarbons through

745 personal air sampling and urinary biomonitoring, *Journal of Environmental Monitoring*, 12,
746 1110-1118, <https://doi.org/10.1039/c000689k>, 2010.

747 Lin, Y., Ma, Y. Q., Qiu, X. H., Li, R., Fang, Y. H., Wang, J. X., Zhu, Y. F., Hu, D.: Sources, transformation,
748 and health implications of PAHs and their nitrated, hydroxylated, and oxygenated derivatives in
749 PM_{2.5} in Beijing, *Journal of Geophysical Research-Atmospheres*, 120, 7219-7228,
750 <https://doi.org/10.1002/2015jd023628>, 2015.

751 **Lin, Y., Shi, X. D., Qiu, X. H., Jiang, X., Liu, J. M., Zhong, P. W., Ge, Y. H., Tseng, C.-H., Zhang, J.**
752 **F., Zhu, T., Araujo, J. A., Zhu, Y. F.: Reduction in polycyclic aromatic hydrocarbon**
753 **exposure in Beijing following China ' s clean air actions. *Science Bulletin*,**
754 **<https://doi.org/10.1016/j.scib.2024.08.015>, 2024.**

755 Liu, S. J., Lu, Y. L., Wang, T. Y., Xie, S. W., Jones, K. C., Sweetman, A. J.: Using gridded multimedia
756 model to simulate spatial fate of Benzo α pyrene on regional scale, *Environment International*,
757 63, 53-63, <https://doi.org/10.1016/j.envint.2013.10.015>, 2014.

758 Lou, S. J., Shrivastava, M., Ding, A. J., Easter, R. C., Fast, J. D., Rasch, P. J., Shen, H. Z., Simonich, S.
759 M., Smith, S. J., Tao, S., Zelenyuk, A.: Shift in Peaks of PAH-Associated Health Risks From
760 East Asia to South Asia and Africa in the Future, *Earths Future*, 11, 15,
761 <https://doi.org/10.1029/2022ef003185>, 2023.

762 Ma, W. L., Liu, L. Y., Jia, H. L., Yang, M., Li, Y. F.: PAHs in Chinese atmosphere Part I: Concentration,
763 source and temperature dependence, *Atmospheric Environment*, 173, 330-337,
764 <https://doi.org/10.1016/j.atmosenv.2017.11.029>, 2018.

765 Ma, W. L., Zhu, F. J., Liu, L. Y., Jia, H. L., Yang, M., Li, Y. F.: PAHs in Chinese atmosphere Part II: Health
766 risk assessment, *Ecotoxicology and Environmental Safety*, 200, 9,
767 <https://doi.org/10.1016/j.ecoenv.2020.110774>, 2020.

768 Mu, Q., Shiraiwa, M., Octaviani, M., Ma, N., Ding, A. J., Su, H., Lammel, G., Pöschl, U., Cheng, Y. F.:
769 Temperature effect on phase state and reactivity controls atmospheric multiphase chemistry and
770 transport of PAHs, *Science Advances*, 4, 8, <https://doi.org/10.1126/sciadv.aap7314>, 2018.

771 Nam, K. J., Li, Q., Heo, S. K., Tariq, S., Loy-Benitez, J., Woo, T. Y., Yoo, C. K.: Inter-regional multimedia
772 fate analysis of PAHs and potential risk assessment by integrating deep learning and climate
773 change scenarios, *Journal of Hazardous Materials*, 411, 12,

774 <https://doi.org/10.1016/j.jhazmat.2021.125149>, 2021.

775 Octaviani, M., Tost, H., Lammel, G.: Global simulation of semivolatile organic compounds - development
776 and evaluation of the MESSy submodel SVOC (v1.0), *Geoscientific Model Development*, 12,
777 3585-3607, <https://doi.org/10.5194/gmd-12-3585-2019>, 2019.

778 Odabasi, M., Cetin, E., Sofuoglu, A.: Determination of octanol–air partition coefficients and supercooled
779 liquid vapor pressures of PAHs as a function of temperature: Application to gas–particle
780 partitioning in an urban atmosphere, *Atmospheric Environment*, 40, 6615-6625,
781 <https://doi.org/10.1016/j.atmosenv.2006.05.051>, 2006.

782 Quan, J. N., Tie, X. X., Zhang, Q., Liu, Q., Li, X., Gao, Y., Zhao, D. L.: Characteristics of heavy aerosol
783 pollution during the 2012-2013 winter in Beijing, China, *Atmospheric Environment*, 88, 83-89,
784 <https://doi.org/10.1016/j.atmosenv.2014.01.058>, 2014.

785 Ravindra, K., Sokhi, R., Van Grieken, R.: Atmospheric polycyclic aromatic hydrocarbons: Source
786 attribution, emission factors and regulation, *Atmospheric Environment*, 42, 2895-2921,
787 <https://doi.org/10.1016/j.atmosenv.2007.12.010>, 2008.

788 San José, R., Pérez, J. L., Callén, M. S., López, J. M., Mastral, A.: BaP (PAH) air quality modelling
789 exercise over Zaragoza (Spain) using an adapted version of WRF-CMAQ model,
790 *Environmental Pollution*, 183, 151-158, <https://doi.org/10.1016/j.envpol.2013.02.025>, 2013.

791 Seigneur, C., Karamchandani, P., Lohman, K., Vijayaraghavan, K., Shia, R. L.: Multiscale modeling of
792 the atmospheric fate and transport of mercury, *Journal of Geophysical Research-Atmospheres*,
793 106, 27795-27809, <https://doi.org/10.1029/2000jd000273>, 2001.

794 Semeena, V. S., Lammel, G.: The significance of the grasshopper effect on the atmospheric distribution
795 of persistent organic substances, *Geophysical Research Letters*, 32, 5,
796 <https://doi.org/10.1029/2004gl022229>, 2005.

797 Shen, H. Z., Tao, S., Liu, J. F., Huang, Y., Chen, H., Li, W., Zhang, Y. Y., Chen, Y. C., Su, S., Lin, N., Xu,
798 Y. Y., Li, B. G., Wang, X. L., Liu, W. X.: Global lung cancer risk from PAH exposure highly
799 depends on emission sources and individual susceptibility, *Scientific Reports*, 4, 8,
800 <https://doi.org/10.1038/srep06561>, 2014.

801 Shrivastava, M., Lou, S., Zelenyuk, A., Easter, R. C., Corley, R. A., Thrall, B. D., Rasch, P. J., Fast, J. D.,
802 Simonich, S. L. M., Shen, H. Z., Tao, S.: Global long-range transport and lung cancer risk from

803 polycyclic aromatic hydrocarbons shielded by coatings of organic aerosol, Proceedings of the
804 National Academy of Sciences of the United States of America, 114, 1246-1251,
805 <https://doi.org/10.1073/pnas.1618475114>, 2017.

806 Skamarock, W. C., Klemp, J. B., Dudhia, J., Gill, D., Barker, D. M., Duda, M. G., Huang, X.-Y., Wang,
807 W., Powers, J. G. A Description of the Advanced Research WRF Version 3. 2008.

808 Smith, R. L., Davis, J. M., Speckman, P.: Assessing the human health risk of atmospheric particles,
809 Novartis Found Symp, 220, 59-72; discussion 72-9,
810 <https://doi.org/10.1002/9780470515600.ch4>, 1999.

811 Stockwell, W. R., Middleton, P., Chang, J. S., Tang, X. Y.: The Second Generation Regional Acid
812 Deposition Model Chemical Mechanism for Regional Air Quality Modeling, Journal of
813 Geophysical Research-Atmospheres, 95, 16343-16367,
814 <https://doi.org/10.1029/JD095iD10p16343>, 1990.

815 Strand, A., Hov, O.: A model strategy for the simulation of chlorinated hydrocarbon distributions in the
816 global environment, Water Air and Soil Pollution, 86, 283-316,
817 <https://doi.org/10.1007/bf00279163>, 1996.

818 Su, C., Zheng, D. F., Zhang, H., Liang, R. Y.: The past 40 years' assessment of urban-rural differences in
819 Benzo a pyrene contamination and human health risk in coastal China, Science of the Total
820 Environment, 901, 9, <https://doi.org/10.1016/j.scitotenv.2023.165993>, 2023.

821 van Noort, P. C. M.: A thermodynamics-based estimation model for adsorption of organic compounds by
822 carbonaceous materials in environmental sorbents, Environmental Toxicology and Chemistry,
823 22, 1179-1188, 2003.

824 Walcek, C. J., Aleksic, N. M.: A simple but accurate mass conservative, peak-preserving, mixing ratio
825 bounded advection algorithm with Fortran code, Atmospheric Environment, 32, 3863-3880,
826 [https://doi.org/10.1016/s1352-2310\(98\)00099-5](https://doi.org/10.1016/s1352-2310(98)00099-5), 1998.

827 Wang, L., Zhang, F. Y., Pilot, E., Yu, J., Nie, C. J., Holdaway, J., Yang, L. S., Li, Y. H., Wang, W. Y.,
828 Vardoulakis, S., Krafft, T.: Taking Action on Air Pollution Control in the Beijing-Tianjin-Hebei
829 (BTH) Region: Progress, Challenges and Opportunities, International Journal of Environmental
830 Research and Public Health, 15, 27, <https://doi.org/10.3390/ijerph15020306>, 2018.

831 Wang, Y. S., Li, W. J., Gao, W. K., Liu, Z. R., Tian, S. L., Shen, R. R., Ji, D. S., Wang, S., Wang, L. L.,

832 Tang, G. Q., Song, T., Cheng, M. T., Wang, G. H., Gong, Z. Y., Hao, J. M., Zhang, Y. H.: Trends
833 in particulate matter and its chemical compositions in China from 2013-2017, *Science China-*
834 *Earth Sciences*, 62, 1857-1871, <https://doi.org/10.1007/s11430-018-9373-1>, 2019.

835 Wang, Z. F., Maeda, T., Hayashi, M., Hsiao, L. F., Liu, K. Y.: A nested air quality prediction modeling
836 system for urban and regional scales: Application for high-ozone episode in Taiwan, *Water Air*
837 *and Soil Pollution*, 130, 391-396, <https://doi.org/10.1023/a:1013833217916>, 2001.

838 Wang, Z. X., Li, J. X., Mu, X., Zhao, L. Y., Gu, C., Gao, H., Ma, J. M., Mao, X. X., Huang, T.: A WRF-
839 CMAQ modeling of atmospheric PAH cycling and health risks in the heavy petrochemical
840 industrialized Lanzhou valley, Northwest China, *Journal of Cleaner Production*, 291, 9,
841 <https://doi.org/10.1016/j.jclepro.2021.125989>, 2021.

842 Wei, Y., Chen, X. S., Chen, H. S., Li, J., Wang, Z. F., Yang, W. Y., Ge, B. Z., Du, H. Y., Hao, J. Q., Wang,
843 W., Li, J. J., Sun, Y. L., Huang, H. L.: IAP-AACM v1.0: a global to regional evaluation of the
844 atmospheric chemistry model in CAS-ESM, *Atmospheric Chemistry and Physics*, 19, 8269-
845 8296, <https://doi.org/10.5194/acp-19-8269-2019>, 2019.

846 Wu, Z. C., Chen, X. S., and Wang, Z. F.: A Global-Regional Nested Model of Polycyclic aromatic
847 hydrocarbons, Zenodo [code], <https://doi.org/10.5281/zenodo.12214119>, 2024.

848 Wu, Z. C., Chen, X. S., and Wang, Z. F.: Results and validation of Global-Regional Nested Model for
849 polycyclic aromatic hydrocarbons., Zenodo [data set],
850 <https://doi.org/10.5281/zenodo.11595165>, 2024.

851 Yan, D. H., Wu, S. H., Zhou, S. L., Tong, G. J., Li, F. F., Wang, Y. M., Li, B. J.: Characteristics, sources
852 and health risk assessment of airborne particulate PAHs in Chinese cities: A review,
853 *Environmental Pollution*, 248, 804-814, <https://doi.org/10.1016/j.envpol.2019.02.068>, 2019.

854 **Yang, L., Zhang, X., Xing, W.L., Zhou, Q.Y., Zhang, L.L., Wu, Q., Zhou, Z.J., Chen, R.J., Toriba,**
855 **A., Hayakawa, K., Tang, N.: Yearly variation in characteristics and health risk of**
856 **polycyclic aromatic hydrocarbons and nitro-PAHs in urban shanghai from 2010-2018.**
857 ***Journal of Environmental Sciences*, 99, 72-79, <https://doi.org/10.1016/j.jes.2020.06.017>,**
858 **2021.**

859 Ye, Q., Li, J., Chen, X., Chen, H., Yang, W., Du, H., Pan, X., Tang, X., Wang, W., Zhu, L., Li, J., Wang,
860 Z., Wang, Z.: High-resolution modeling of the distribution of surface air pollutants and their

861 intercontinental transport by a global tropospheric atmospheric chemistry source–receptor
862 model (GNAQPMS-SM), *Geoscientific Model Development*, 14, 7573-7604,
863 <https://doi.org/10.5194/gmd-14-7573-2021>, 2021.

864 Zaveri, R. A., Peters, L. K.: A new lumped structure photochemical mechanism for large-scale
865 applications, *Journal of Geophysical Research-Atmospheres*, 104, 30387-30415,
866 <https://doi.org/10.1029/1999jd900876>, 1999.

867 **Zhang, H., Zhang, X., Wang, Y., Bai, P.C., Zhang, L.L., Chen, L.J., Han, C., Yang, W.J., Wang,**
868 **Q.M., Cai, Y.P., Nagao, S., Tang, N.: Factor analysis of recent variations of atmospheric**
869 **polycyclic aromatic hydrocarbons (PAHs) and 1-nitropyrene (1-NP) in Shenyang, China**
870 **from 2014 to 2020. *Atmospheric Pollution Research*, 14, 8,**
871 **<https://doi.org/10.1016/j.apr.2023.101900>, 2023.**

872 **Zhang, J.W., Feng, L.H., Zhao, Y., Hou, C.C., Gu, Q.: Health risks of PM2.5-bound polycyclic**
873 **aromatic hydrocarbon (PAH) and heavy metals (PPAH&HM) during the replacement of**
874 **central heating with urban natural gas in Tianjin, China. *Environ. Geochem. Health*, 44,**
875 **2495-2514, <https://doi.org/10.1007/s10653-021-01040-8>, 2022.**

876 Zhang, L., Brook, J. R., Vet, R.: A revised parameterization for gaseous dry deposition in air-quality
877 models, *Atmospheric Chemistry and Physics*, 3, 2067-2082, [https://doi.org/10.5194/acp-3-](https://doi.org/10.5194/acp-3-2067-2003)
878 [2067-2003](https://doi.org/10.5194/acp-3-2067-2003), 2003.

879 Zhang, M., Xie, J. F., Wang, Z. T., Zhao, L. J., Zhang, H., Li, M.: Determination and source identification
880 of priority polycyclic aromatic hydrocarbons in PM2.5 in Taiyuan, China, *Atmospheric*
881 *Research*, 178, 401-414, <https://doi.org/10.1016/j.atmosres.2016.04.005>, 2016.

882 Zhang, Q., Zheng, Y. X., Tong, D., Shao, M., Wang, S. X., Zhang, Y. H., Xu, X. D., Wang, J. N., He, H.,
883 Liu, W. Q., Ding, Y. H., Lei, Y., Li, J. H., Wang, Z. F., Zhang, X. Y., Wang, Y. S., Cheng, J., Liu,
884 Y., Shi, Q. R., Yan, L., Geng, G. N., Hong, C. P., Li, M., Liu, F., Zheng, B., Cao, J. J., Ding, A.
885 J., Gao, J., Fu, Q. Y., Huo, J. T., Liu, B. X., Liu, Z. R., Yang, F. M., He, K. B., Hao, J. M.: Drivers
886 of improved PM2.5 air quality in China from 2013 to 2017, *Proceedings of the National*
887 *Academy of Sciences of the United States of America*, 116, 24463-24469,
888 <https://doi.org/10.1073/pnas.1907956116>, 2019.

889 Zhang, Y., Hemperly, J., Meskhidze, N., Skamarock, W. C.: The Global Weather Research and

890 Forecasting (GWRP) Model: Model Evaluation, Sensitivity Study, and Future Year Simulation,
891 Atmospheric and Climate Sciences, 2, 231-253, <https://doi.org/10.4236/acs.2012.23024>, 2012a.

892 Zhang, Y., Jaeglé, L., van Donkelaar, A., Martin, R. V., Holmes, C. D., Amos, H. M., Wang, Q., Talbot,
893 R., Artz, R., Brooks, S., Luke, W., Holsen, T. M., Felton, D., Miller, E. K., Perry, K. D., Schmeltz,
894 D., Steffen, A., Tordon, R., Weiss-Penzias, P., Zsolway, R.: Nested-grid simulation of mercury
895 over North America, Atmospheric Chemistry and Physics, 12, 6095-6111,
896 <https://doi.org/10.5194/acp-12-6095-2012>, 2012b.

897 Zhang, Y., Shen, H., Tao, S., Ma, J.: Modeling the atmospheric transport and outflow of polycyclic
898 aromatic hydrocarbons emitted from China, Atmospheric Environment, 45, 2820-2827,
899 <https://doi.org/10.1016/j.atmosenv.2011.03.006>, 2011a.

900 Zhang, Y., Tao, S., Ma, J., Simonich, S.: Transpacific transport of benzo[a]pyrene emitted from Asia,
901 Atmospheric Chemistry and Physics, 11, 11993-12006, [https://doi.org/10.5194/acp-11-11993-](https://doi.org/10.5194/acp-11-11993-2011)
902 2011, 2011b.

903 Zhang, Y. X., Tao, S.: Global atmospheric emission inventory of polycyclic aromatic hydrocarbons (PAHs)
904 for 2004, Atmospheric Environment, 43, 812-819,
905 <https://doi.org/10.1016/j.atmosenv.2008.10.050>, 2009.

906 Zhang, Y. X., Tao, S., Shen, H. Z., Ma, J. M.: Inhalation exposure to ambient polycyclic aromatic
907 hydrocarbons and lung cancer risk of Chinese population, Proceedings of the National Academy
908 of Sciences of the United States of America, 106, 21063-21067,
909 <https://doi.org/10.1073/pnas.0905756106>, 2009.

910 Zhen, Z. X.: Observation and simulation of atmospheric polycyclic aromatic hydrocarbons in the North
911 China Plain, Ph.D.thesis, Nanjing university of information science and technology, China, 142
912 pp., 2023.

913 Zhu, F. J., Ma, W. L., Hu, P. T., Zhang, Z. F., Li, Y. F.: Temporal trends of atmospheric PAHs: Implications
914 for the influence of the clean air action, Journal of Cleaner Production, 296, 8,
915 <https://doi.org/10.1016/j.jclepro.2021.126494>, 2021.